# 学位論文（要約）

**Study on 3-D Velocity Structure of an Accretionary Wedge and its Effects on the Seismic Wavefield of Offshore Earthquakes**

（付加体の三次元速度構造と海域地震の波動場への影響に関する研究）

平成 28 年 12 月博士（理学）申請

東京大学大学院理学系研究科
地球惑星科学専攻

郭　雨 佳

# Abstract

A thick, low-velocity accretionary wedge overlying a subducting oceanic plate significantly affects the ground motions of offshore earthquakes. To enable more reliable ground-motion predictions and accurately estimate seismic sources during offshore earthquakes, it is important to clarify the detailed 3-D velocity structure of the accretionary wedge and investigate its effects on the propagation of seismic waves.

To estimate 3-D subsurface velocity structures such as accretionary wedges, we proposed a nonlinear inversion method of full-waveform data. Our inversion method included an efficient approach, in which the higher-frequency components of data are gradually incorporated; thus, velocity structures are estimated with increasingly short scale lengths. We performed synthetic tests and showed that waveform inversion incorporating this approach can greatly reduce the waveform residual at a relatively low 3-D computational cost. Subsequently, using this inversion method, we improved a 3-D velocity structure model of the accretionary wedge along the Nankai Trough, off the southwest of Japan, where the occurrence potential of a forthcoming subduction earthquake is high. The waveform data recorded by ocean-bottom observation networks as well as onshore networks were utilized in our inversion. When updated by the waveform inversion, the 3-D velocity structure model of the accretionary wedge showed thicker low-velocity layers than those based on seismic surveys. We also validated the updated model and confirmed that it can reproduce the observed data reasonably well.

To evaluate the effects of the accretionary wedge along the Nankai Trough on ground motions of the land area, we performed 3-D ground motion simulations for numerous seismic sources using the updated velocity structure model. The simulation results demonstrated that the accretionary wedge has the effect of decreasing the peak amplitude and elongating the duration of ground motions. These effects depend significantly on source location. We

suggest that large later phases, which contribute to the elongation of ground motions, originate mainly from basin-induced surface waves excited at the boundary between the accretionary wedge and the crust near the trough axis. We also found that the accretionary wedge traps only short-period (< 10 s) waves and efficiently transmits long-period (> 10 s) waves toward the land area. Our finding can explain the predominant period of ground motions observed at the land area. Moreover, we found that the amplitude reduction of Rayleigh waves caused by seawater occurs at periods longer than those in the case of the absence of the accretionary wedge. In offshore areas with an accretionary wedge, we suggest that higher-mode surface waves are more important to ground motions in the land area than are fundamental-mode surface waves.

To examine the effects of the accretionary wedge on source analyses, we also estimated the rupture process of the 1944 Tonankai earthquake by the inversion of its strong-motion data. In this inversion, the updated velocity structure model was used to calculate 3-D Green's functions. The inversion result shows that a shallow slip occurred off the Kii Peninsula, which has not been clarified by studies using 1-D Green's functions. We suggest that owing to the de-amplification effect of the accretionary wedge on ground motions at the land area, source inversions using 1-D Green's functions or 3-D Green's functions without considering this effect result in underestimation of the seismic moment and the maximum slip.

# Contents

# Chapter 1
# Introduction

## 1.1 Background and objective

Great subduction earthquakes have the potential to efficiently generate ground motions because of their large magnitudes and shallow depths. The generated ground motions are then significantly influenced by the various effects of 3-D velocity structures and are often observed with large amplitudes and long durations. As a consequence, ground motions during great subduction earthquakes can cause serious damage. For example, the 1985 Michoacan, Mexico, earthquake ($M_w$ 8.0) along the Middle America Trench killed about 20,000 people and demolished many buildings in Mexico City (Anderson *et al.*, 1986; Beck and Hall, 1986).

Because 3-D velocity structures, such as sedimentary basins, in land areas usually have major effects on ground motions, 3-D velocity structures in such areas have been the focus of numerous studies (e.g., Furumura and Koketsu, 1998; Koketsu and Kikuchi, 2000; Graves and Wald, 2004; Aoi *et al.*, 2008). However, because ground motions for subduction earthquakes propagate through offshore areas with a long path length, several studies (e.g., Furumura and Singh, 2002) have also suggested that the effects of 3-D velocity structures in offshore areas should be carefully investigated.

Accretionary wedges (thick oceanic sediments) affect ground motions during subduction earthquakes. They overlie subducting oceanic plates with gentle subduction angles, such as the Cascadia (e.g., Olsen *et al.*, 2008), south Chilean (e.g., Haberland *et al.*, 2009), and Sumatra-Andaman (e.g., Harmon *et al.*, 2012) subduction zones. The effects of such oceanic sediments on ground motions were first investigated by Shapiro *et al.* (1998).

In Japan, the Nankai Trough (Fig. 1) is a subduction zone with an accretionary wedge (e.g., Nakanishi *et al.*, 1998). There are several studies that examined the effects of the accretionary

wedge along the Nankai Trough on ground motions. Yamada and Iwata (2005) and Yoshimura *et al.* (2008) performed 3-D ground motion simulations during the largest foreshock ($M_w$ 7.2; Fig. 1) of the 2004 off the Kii Peninsula earthquake and concluded that the accretionary wedge decreased the peak amplitude and prolonged the duration of ground motions at the land area. Watanabe *et al.* (2014) and Goto and Nagano (2015) confirmed these effects and suggested that the accretionary wedge in the offshore area can significantly trap seismic waves. On the other hand, several studies showed opposite effects. Furumura *et al.* (2008) performed 3-D ground motion simulations during the 1944 Tonankai earthquake ($M_w$ 8.1; Fig. 1) and the 2004 off the Kii Peninsula earthquake ($M_w$ 7.4; Fig. 1), and pointed out that the accretionary wedge produces an amplification effect by efficiently guiding seismic waves toward the land area. This effect was confirmed by Ikegami *et al.* (2008). Supporting Furumura *et al.* (2008) and Ikegami *et al.* (2008), Petukhin *et al.* (2016) showed that the accretionary wedge can considerably amplify surface waves.

The conflicting results suggested by these studies are mainly attributed to differences in velocity structure models used for ground motion simulations. The velocity structure models assumed by these studies were not based on seismic surveys in the offshore area, and the seismic velocities and geometries of the accretionary wedge differed among studies. For example, the seismic velocity of the accretionary wedge in the velocity structure model of Furumura *et al.* (2008) was relatively high. On the other hand, Yoshimura *et al.* (2008) used a velocity structure model with a thicker and lower-velocity accretionary wedge than Furumura *et al.* (2008). These examples demonstrate that results relating to the effects of an accretionary wedge significantly depend on the velocity structure model used for the accretionary wedge.

To accurately evaluate the effects of the accretionary wedge, 3-D velocity structure models of the accretionary wedge that are based on seismic surveys and have high reliability are required. Recently, Nakamura *et al.* (2014a, 2015) performed ground motion simulations using a 3-D velocity structure model based on seismic surveys in the offshore area. They

showed that although the accretionary wedge significantly affects ground motions at periods of less than ~20 s, the 3-D velocity structure model has a relatively low accuracy at less than ~10 s. Guo *et al.* (2016) also validated a 3-D velocity structure model compiled based on seismic surveys and pointed out the need to improve velocity structure models of the accretionary wedge using both onshore and offshore observations.

The velocity structure models constructed on the basis of seismic surveys usually consider only the travel time of seismic waves. To explain the amplitude and spectral features as well as the travel time, improvements in velocity structure models using various types of data, e.g., horizontal-to-vertical (H/V) spectral ratios, are required (Koketsu *et al.*, 2009). The time histories of observed waveforms are the most effective form of data for such improvements because they directly include the complex effects of 3-D velocity structures. Therefore, in this study, we propose an inversion method of full-waveform data for 3-D velocity structures. We introduce a multiscale approach to the method. As detailed in Chapter 2, this approach can overcome problems associated with the initial estimate required for the inversion as well as the computational cost of 3-D forward simulations. Next, we apply this method to the estimation of the 3-D velocity structure of the accretionary wedge in the Tonankai region, where the 1944 Tonankai earthquake occurred. Our waveform inversion uses time-history waveforms recorded by an ocean-bottom observation network installed inside the accretionary wedge as well as the onshore observation network. Then, using the 3-D velocity structure model improved by the waveform inversion, we perform 3-D ground motion simulations to evaluate the effects of the accretionary wedge on ground motions at the land area.

In hypocenter determination, magnitude estimation, and rupture process modeling of offshore earthquakes along the Nankai Trough, it is also important to consider the effects of the accretionary wedge (Nakamura *et al.*, 2015). On the basis that ground motions in the offshore area are significantly amplified by sediments of the accretionary wedge, Hayashimoto and Hoshiba (2013) and Nakamura *et al.* (2014a) demonstrated that the

magnitude estimate based on offshore observations can lead to a large overestimation. Moreover, Obana *et al.* (2009) and Nakano *et al.* (2015) demonstrated that in hypocenter determination based on offshore observations, the use of 3-D velocity structure models with the accretionary wedge can provide more accurate estimations of source locations. These studies focused mainly on offshore observations. Although source analyses with offshore observations will be widely used, records obtained by ocean bottom seismometers often suffer from long-period noises, strong nonlinear effects, and scale-out caused by intense shakes during large earthquakes (e.g., Yamamoto *et al.*, 2004; Hayashimoto and Hoshiba, 2013; Kobayashi and Araki, 2016). Consequently, offshore observations alone can deleteriously affect source analyses, and their combined use with onshore observations is reasonable. Nevertheless, few studies have demonstrated the effects of the accretionary wedge on source analyses based on onshore observations.

Because the occurrence potential of a forthcoming subduction earthquake along the Nankai Trough is high (Headquarters for Earthquake Research Promotion, 2013), an insight into the effects of the accretionary wedge on source analyses based on onshore observations is essential. To achieve this goal, we also attempt to estimate the rupture process of the 1944 Tonankai earthquake, which was one of the most recent great subduction earthquakes, using the 3-D velocity structure model with the accretionary wedge. The rupture process estimated by appropriately incorporating the effects of the accretionary wedge can play an important role not only in better understanding the generation mechanism of recurring subduction earthquakes but also in accurately predicting ground motions for future events.

## 1.2 Structure of this study

This study consists of five chapters. The current chapter serves as an introduction.

Chapter 2 presents the waveform inversion with the multiscale approach for the 3-D velocity structure of an accretionary wedge. First, we describe our inversion method. Next,

we perform synthetic tests to confirm the validity of the method. Then, we estimate the 3-D velocity structure of the accretionary wedge by applying the method to real data. Finally, we validate our velocity structure model and compare it with the previous studies.

Chapter 3 clarifies the effects of the accretionary wedge on ground motions at the land area. We evaluate these effects by performing 3-D ground motion simulations for numerous seismic sources, in which the velocity structure model provided in Chapter 2 is used. We also discuss several important propagation mechanisms associated with the effects.

In Chapter 4, we estimate the rupture process of the 1944 Tonankai earthquake by the waveform inversion of strong-motion data; 3-D Green's functions are used for the estimation, which provide better accuracy than 1-D Green's functions used in previous studies. In calculating 3-D Green's functions, the velocity structure model updated by the waveform inversion of Chapter 2 is also utilized. We also discuss the relationships between the slip distribution and crustal structures.

Chapter 5 presents the conclusions of this study.

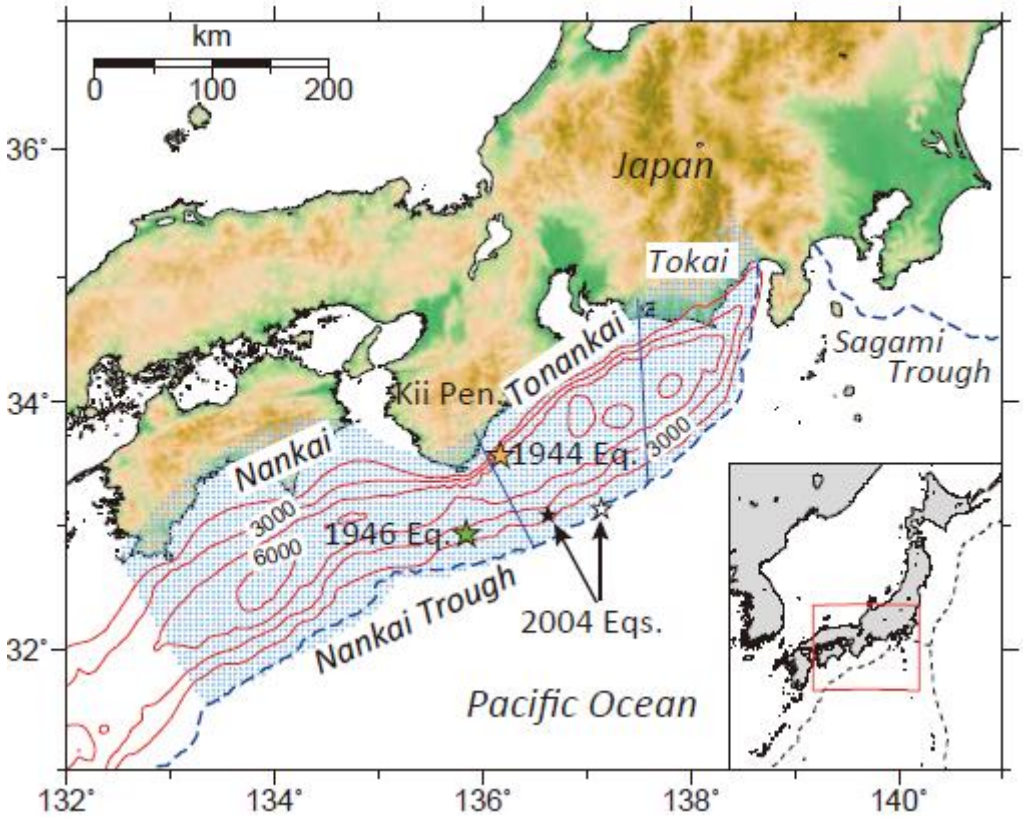


Figure 1　Map of the Nankai Trough. Orange and green stars mark epicenters of the 1944 Tonankai and 1946 Nankai earthquakes. Open and solid stars denote epicenters of the 2004 off the Kii Peninsula earthquake and its largest foreshock, respectively. The aqua-shaded area indicates the source region of subduction earthquakes along the Nankai trough. Two blue lines denote the divisions of the source region. Red contours indicate the thickness of the accretionary wedge in the model of Koketsu *et al.* (2008, 2012).

# Chapter 2

# Waveform inversion for the 3-D velocity structure of an accretionary wedge

第 2 章

本章については、5 年以内に雑誌等で刊行予定のため、非公開。

# Chapter 3
# Effects of the accretionary wedge on ground motions

## 3.1 Introduction

The waveform inversion in Chapter 2 constructed a 3-D velocity structure model of the accretionary wedge along the Nankai Trough. Compared with the model based on seismic surveys, the new model is more suitable for reproducing ground motions. Our model makes it possible to accurately understand and quantitatively evaluate the effects of the accretionary wedge. In this chapter, we perform 3-D ground motion simulations to investigate (i) the effects of the accretionary wedge on ground motions in the land area and (ii) the propagation mechanism associated with such effects. Because subduction earthquakes usually occur in spatially diverse source locations, some previous studies (Shapiro *et al.*, 1998, 2002; Watanabe *et al.*, 2014) have suggested that the effects of the accretionary wedge are likely to be governed by the source location. Taking this suggestion into consideration, we simulate ground motions for numerous seismic sources over a wide offshore area.

## 3.2 Ground motion simulation method

We deployed 780 virtual point sources with spatial intervals of ~5 km to cover the plate boundary in the Tonankai region (Fig. 3.1). Each point source was modeled to release a pure reverse slip (rake = 90°) with a bell-shaped moment rate function with a rise time of 6 s. The assumptions of strike and dip were based on the 3-D geometry of the subducting Philippine Sea plate in the velocity structure model of Koketsu *et al.* (2008, 2012). We calculated velocity waveforms (0.05–0.25 Hz) at three sites (Fig. 3.1) using the 3-D finite-element method with voxel meshes, as in the forward simulations for the waveform inversion in

Chapter 2. The size of the voxel meshes was 200 and 400 m for depths shallower and deeper than 7.4 km, respectively. Topography, ocean water, and constant $Q_P$ and $Q_S$ values over a wide-frequency band were implemented in the calculations. To save computational time, a source-receiver reciprocity method for seismic wavefields was jointly utilized in the simulations, following Graves and Wald (2001).

We defined the effect of the accretionary wedge as the difference in the waveforms simulated in velocity structure models with and without the accretionary wedge. The final model obtained by the waveform inversion in Chapter 2 was used as the velocity structure model with the accretionary wedge. The velocity structure model without the accretionary wedge was generated by replacing the *S*-wave velocities of 0.6, 1.2, and 2.2 km/s (Table 2.3 and Fig. 3.2a) with 2.4 and 3.2 km/s (Table 3.1 and Fig. 3.2b). We evaluated and discussed the effects of the accretionary wedge in terms of amplitude, duration, and period, which are important indicators for ground motions.

## 3.3 Results

For three sites, Figure 3.3 illustrates the ratios of the horizontal peak ground velocities of the model with the accretionary wedge to the model without the accretionary wedge. We can see that the accretionary wedge has the effect of lessening the peak amplitudes of the ground motions. The longer distance the seismic waves travel within the accretionary wedge, the stronger this effect becomes. For example, at site E (Fig. 3.3a), peak ground velocities of the model with the accretionary wedge were only ~20% of those of the model without the accretionary wedge for sources on the eastern edge of the Tonankai region, whereas there were no pronounced differences between the two models for sources closest to E. Figure 3.4 compares differences between the two models in terms of the recorded times of the horizontal peak ground velocities. We can see that the accretionary wedge also has the effect of delaying the recorded times, i.e., elongating the duration of the ground motions. This effect depends on

the source depth rather than the path length in the accretionary wedge. For sources with depths of more than ~10 km, differences between the two models were small; by contrast, for sources with depths of less than ~10 km, the model with the accretionary wedge showed substantial delays (of more than one minute) in the recorded times relative to the model without the accretionary wedge. These delays are associated with the development of later phases in the accretionary wedge. Figure 3.5 shows a comparison of waveforms of the two models at site G for three sources, Q, R, and S (Fig. 3.1), along the profile A–B. For source Q, the waveform of the model with the accretionary wedge indicated an amplitude reduction in the direct wave at a lapse time of ~50 s and prominent later phases. These features are clearly recognized for source Q, and they are sufficiently small to be ignored for source S.

The sources with depths of less than ~10 km lie under the area where sediments of the accretionary wedge initiate thickening similar to that of a basin edge. If we regard the accretionary wedge as a basin, the origin of later phases for source Q can be interpreted to be basin-induced surface waves (e.g., Bard and Bouchon, 1980a, b; Kawase, 2003) excited at the boundary between the accretionary wedge and the crust near the trough axis. Figure 3.6 indicates that basin-induced surface waves with large amplitudes emerge from close to the epicenter, following *S* waves. We suggest that such basin-induced surface waves can play a significant role in elongating the duration of ground motions.

By simulating 2-D microseismic wavefields, Gualtieri *et al.* (2015) implied that the effects of oceanic sediments on ground motions at the land area depend on frequency. In this study, we found that the amplitude reduction caused by the accretionary wedge in the Tonankai region is mainly restricted to periods of less than 10 s (Fig. 3.7). The waveforms in the period range of 4–10 s for source Q (Fig. 3.8a) also support this finding. On the other hand, the waveforms in the periods beyond 10 s for the model with the accretionary wedge had similar peak amplitude and significantly longer duration relative to that of the model without the accretionary wedge (Fig. 3.8b). Therefore, we suggest that the accretionary wedge has the effect of trapping only shorter-period waves and efficiently transmitting longer-period waves

toward the land area.

## 3.4 Discussion

第 3 章第 4 節

本節については、5 年以内に雑誌等で刊行予定のため、非公開。

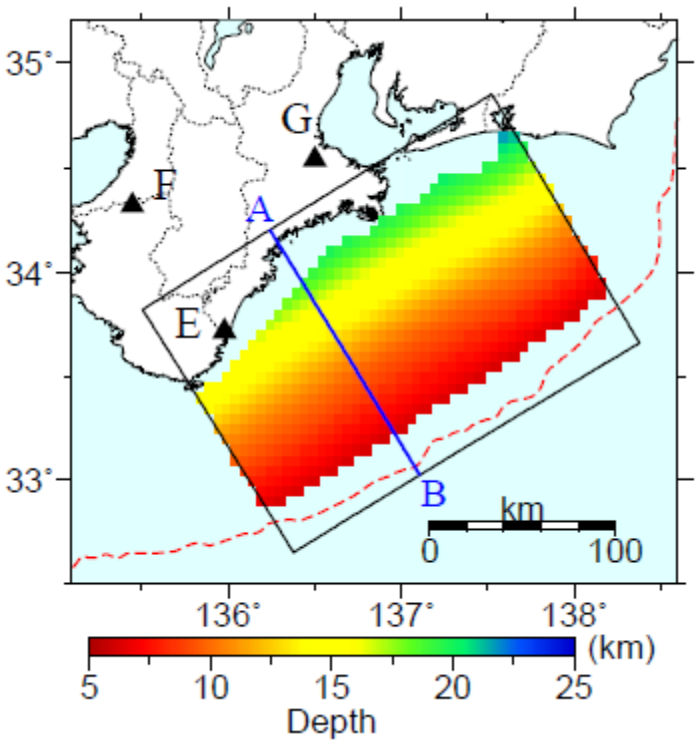


Figure 3.1 Depths of the point sources used to evaluate the effects of the accretionary wedge. The rectangle area and triangles denote the area of the waveform inversion in Chapter 2 and stations, respectively.

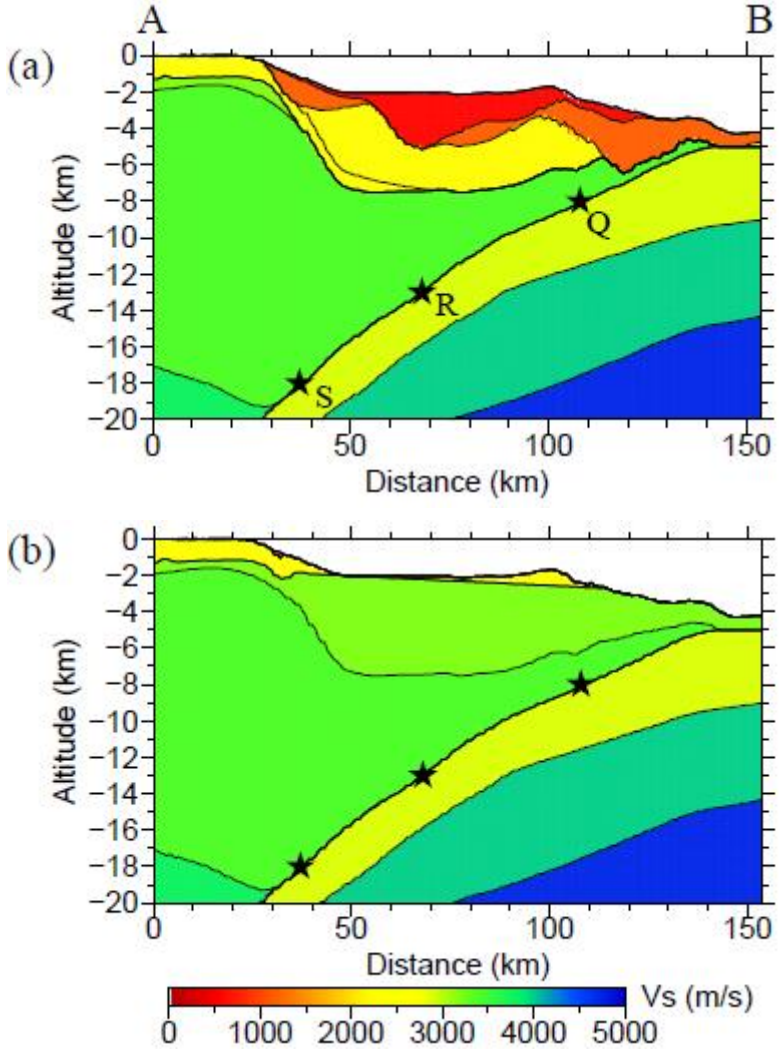


Figure 3.2 Cross-section views of the velocity structure models (a) with and (b) without the accretionary wedge along the profile A–B (Fig. 3.1). The waveforms for sources Q, R, and S are shown in Figure 3.5.

Table 3.1 Physical Parameters of the Two Layers in the Model without the Accretionary Wedge

| Layer No. | *Vp* (km/s) | *Vs* (km/s) | ρ (kg/m$^3$) | $Q_P$ | $Q_S$ |
|---|---|---|---|---|---|
| 1 | 4.2 | 2.4 | 2450 | 680 | 400 |
| 2 | 5.5 | 3.2 | 2650 | 680 | 400 |

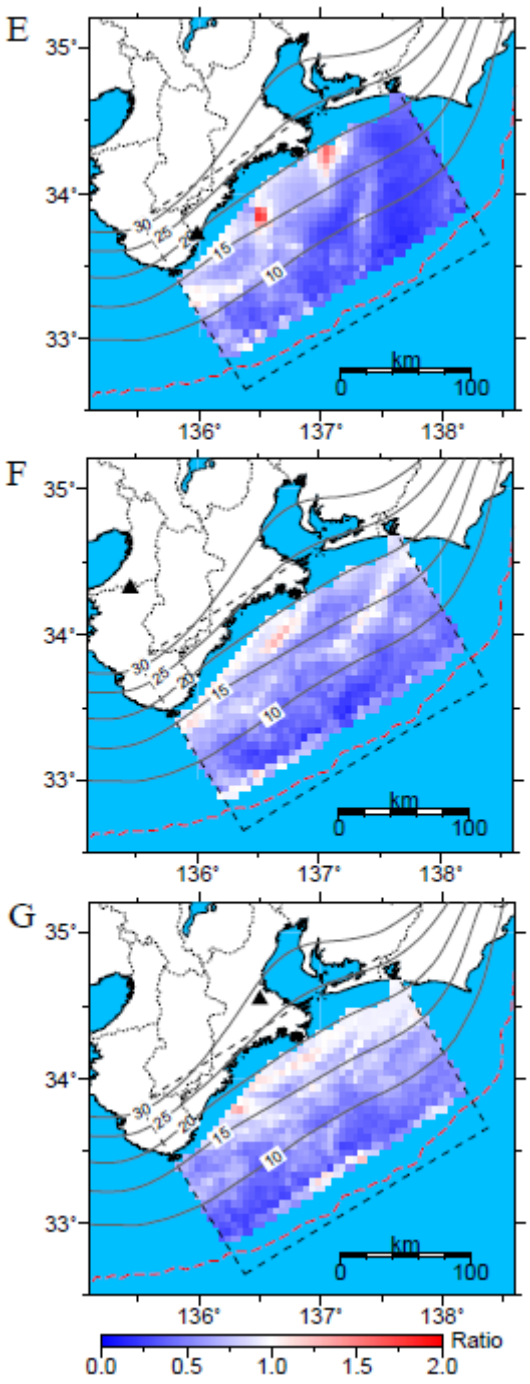


Figure 3.3 Maps of the ratios of the horizontal peak ground velocities of the model with the accretionary wedge to the model without the accretionary wedge for sites E, F, and G. Solid contours mark the depth distribution of the top of the Philippine Sea plate.

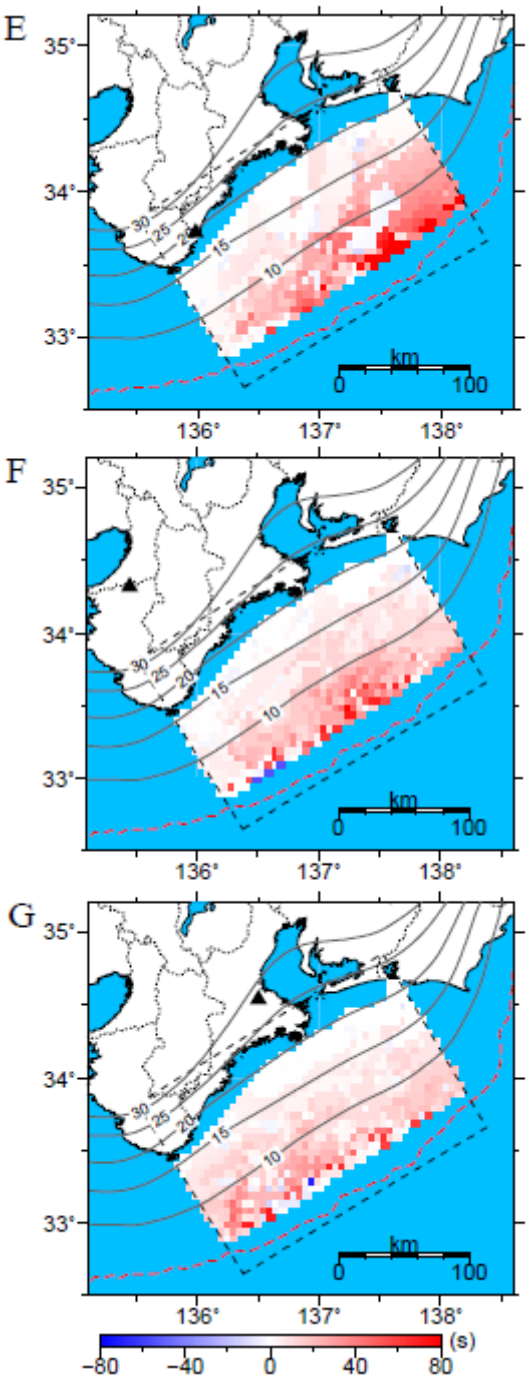


Figure 3.4 Maps of differences between the models with and without the accretionary wedge in terms of the recorded times of the horizontal peak ground velocities for sites E, F, and G. Red means that the record time of the model with the accretionary wedge is more delayed than the model without the accretionary wedge.

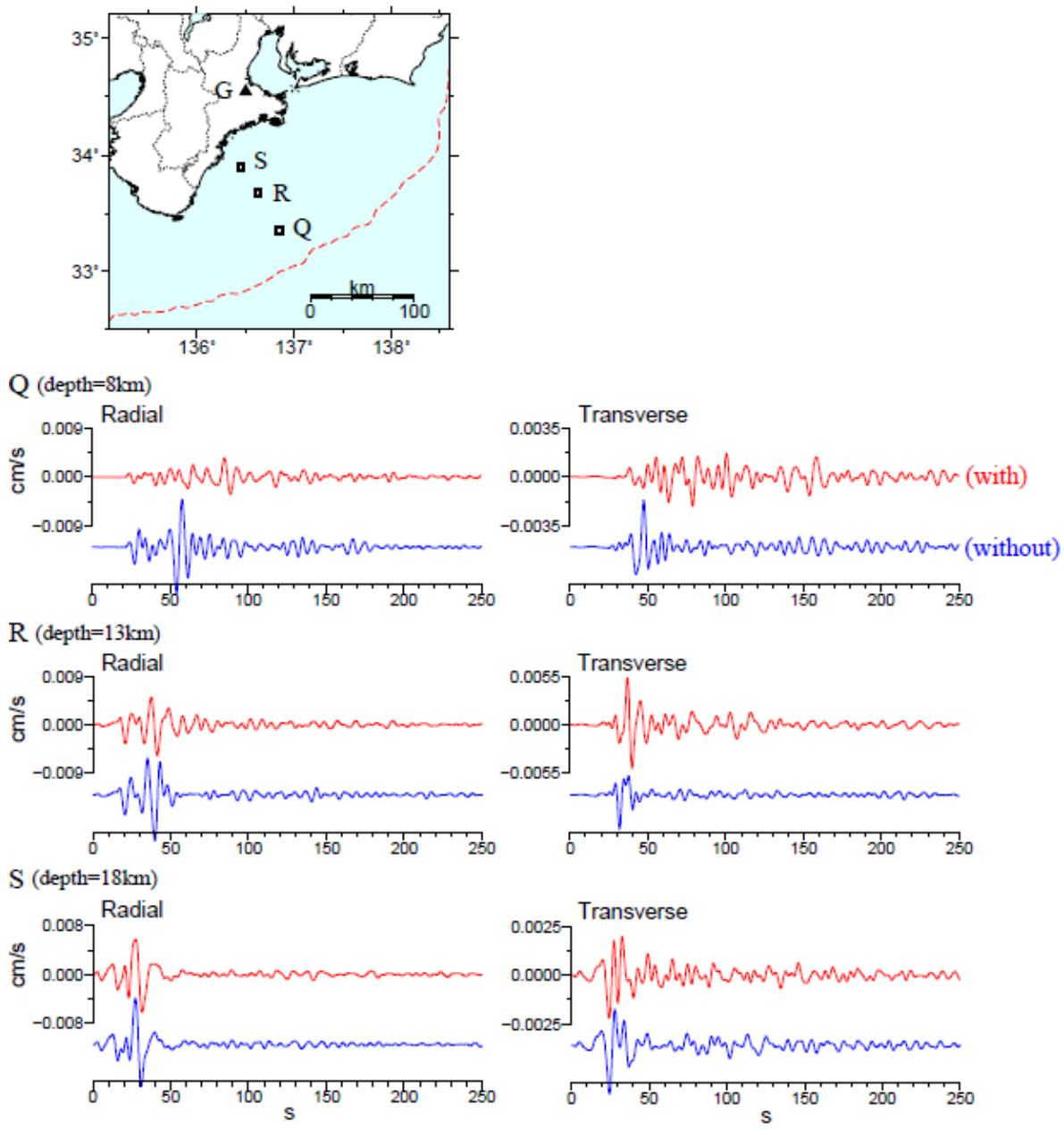


Figure 3.5 Velocity waveforms (0.05–0.25 Hz) of the models with and without the accretionary wedge at site G for sources Q, R, and S.

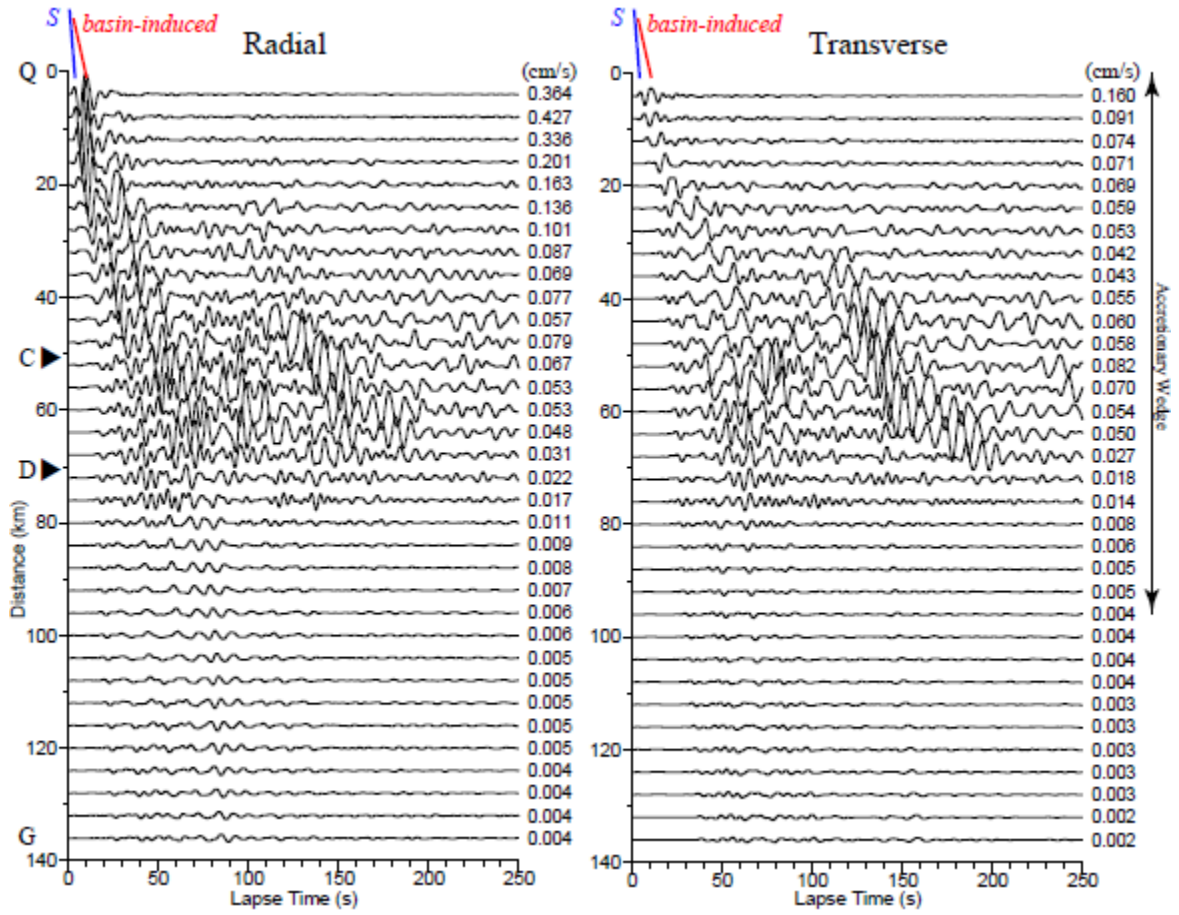


Figure 3.6 Velocity waveforms (0.05–0.25 Hz) along the profile from source Q to site G. The number on the right side of each waveform denotes the peak amplitude.

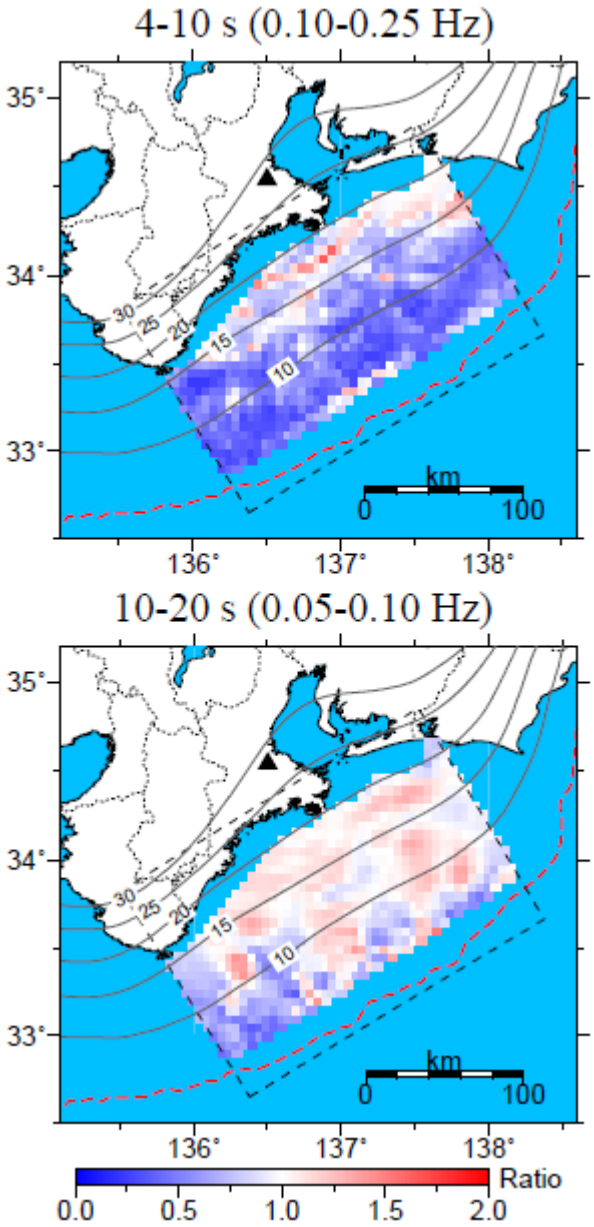


Figure 3.7 Maps of the ratios of the horizontal peak ground velocities of the model with the accretionary wedge to the model without the accretionary wedge in the period ranges of 4–10 and 10–20 s for site G.

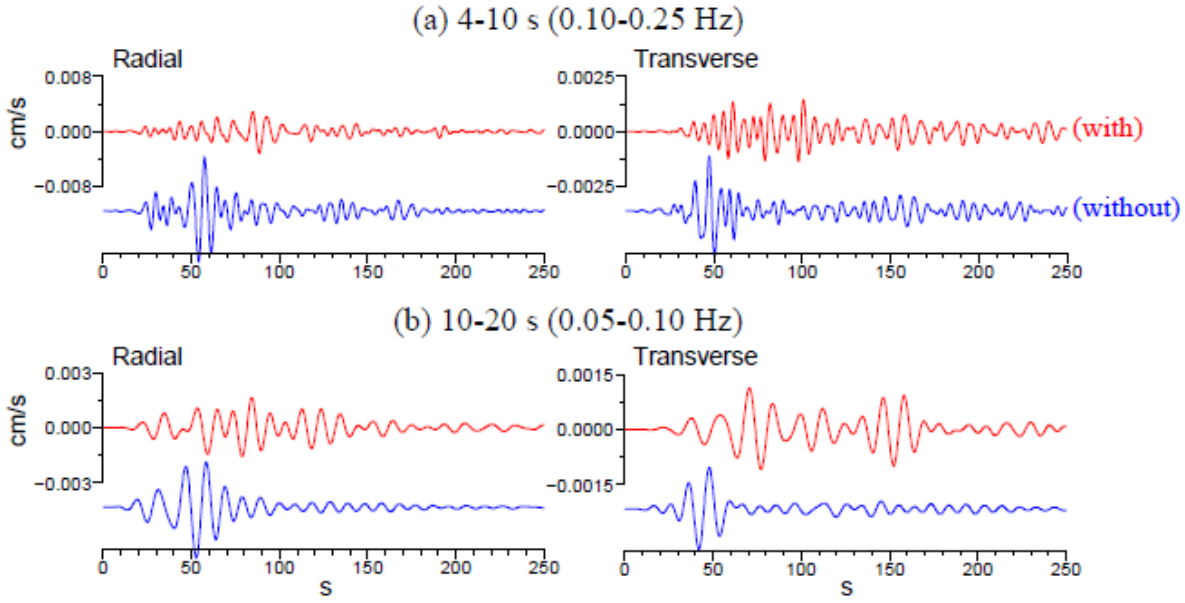


Figure 3.8 Velocity waveforms of the models with and without the accretionary wedge at (a) 4–10 s and (b) 10–20 s at site G for source Q.

Figures 3.9–3.15

図 3.9–3.15

5 年以内に雑誌等で刊行予定のため、非公開。

# Chapter 4
# Source inversion of the 1944 Tonankai earthquake incorporating the effects of the accretionary wedge

## 4.1 Introduction

In Chapter 3, we have revealed the effects of the accretionary wedge on ground motions by performing ground motion simulations. To accurately estimate the rupture processes of offshore earthquakes along the Nankai Trough, these effects should be adequately separated from observed waveforms. Although 1-D velocity structure models are often used for calculating Green's functions in source inversions, 1-D Green's functions cannot incorporate the effects of the accretionary wedge. The use of 3-D Green's functions (e.g., Grave and Wald, 200l; Liu and Archuleta, 2004; Guo *et al.*, 2013) can address this issue. Kagawa *et al.* (2012) also demonstrated the applicability of 3-D Green's functions to source inversions by estimating the rupture process of the 1946 Nankai earthquake (Fig. 1). In this chapter, we estimated the rupture process of the 1944 Tonankai earthquake by the inversion of strong-motion data using 3-D Green's functions calculated for the velocity structure model refined by Chapter 2. The source region of this earthquake roughly coincided with the area of the waveform inversion for 3-D velocity structures of the accretionary wedge in Chapter 2.

There are several previous studies that proposed source models of the 1944 Tonankai earthquake using geodetic data (Sagiya and Thatcher, 1999), tsunami waveform data (Tanioka and Satake, 2001; Baba and Cummins, 2005; Baba *et al.*, 2006), or both (Satake, 1993; Kato and Ando, 1997). These studies suggested a roughly similar slip distribution, i.e., a large slip occurred off the Kii Peninsula, and a medium slip occurred off the Atsumi Peninsula. On the other hand, results estimated using teleseismic and/or strong-motion waveforms (Ichinose *et al.*, 2003; Yamanaka, 2004) suggested that there was no large slip off the Kii Peninsula.

Because strong-motion data are much more sensitive to 3-D velocity structures than other types of data (e.g., Wald and Graves, 2001), the use of 3-D Green's functions can provide a more reliable result.

## 4.2 Method and data

We performed the source inversion using the method of Yoshida *et al.* (1996) and Hikima and Koketsu (2005) based on the formulation of multiple time windows. We assumed a fault plane (210 × 135 $km^2$; Fig. 4.1) based on the aftershock distribution, Nakanishi *et al.* (2002a), and Koketsu *et al.* (2008, 2012). Compared with the studies of Ichinose *et al.* (2003) and Yamanaka (2004), this fault plane fits better with the 3-D geometry of the subducting Philippine Sea plate. The fault plane was divided into 15 × 15 $km^2$ subfaults. The subfaults had different strike and dip angles depending on the 3-D geometry of the subducting Philippine Sea plate. At the shallow part of the fault plane, we did not assume any branching of the fault because the shallow splay fault has sensitivity to tsunamis rather than ground motions (e.g., Park *et al.*, 2002). The slip vector on each subfault was represented by a linear combination of two components in the direction of 90° ±45°, and the time history of each component was represented by five ramp functions with a rise time of 3 s. The epicenter (latitude: 33.70°N, longitude: 136.05°E) and origin time (13:35:39 on December 7, 1944 JST) were based on Kanamori (1972). The rupture velocity for the first time window on each subfault was determined to be 3.0 km/s.

We used displacement waveforms recorded by 14 Central Meteorological Observatory (CMO) stations (Fig. 4.2). These data were digitized and corrected by Ichinose *et al.* (2003) and Yamanaka (2004). All waveforms were bandpass-filtered between 0.05 and 0.25 Hz and re-sampled every 0.5 s. At most stations except KOC and MRT, pendulums went off scale and only the direct waves were available for the inversion. The off-scale amplitudes also made us rely on the waveforms at only stations KOC and MRT, which had long durations, to

estimate the slip at a later stage. Therefore, a slightly strong weight of the spatiotemporal smoothness constraints was adopted to stabilize the inversion.

We calculated 3-D Green's functions using the finite-element method with voxel meshes and the source-receiver reciprocity method for seismic wavefields. The size of the voxel meshes was 200 and 400 m for depths less and greater than 7.0 km, respectively. Topography, ocean water, and constant $Q_P$ and $Q_S$ values over a wide-frequency band were implemented in the calculations. We used the velocity structure model identical to the final model in Chapter 2. A 3-D velocity structure model based on seismic surveys (Guo *et al.*, 2016) was also adopted for the outside of the area of the waveform inversion in Chapter 2. Note that the velocity structure model of the accretionary wedge in such areas, namely in the Nankai and Tokai regions, has not been calibrated owing to the absence of seafloor observations. We included instrumental responses of seismographs in the calculated Green's functions instead of removing instrumental responses from the data.

## 4.3 Results

Figure 4.3 illustrates the slip distribution of the estimated source model. The maximum slip was ~5 m at the southeast of the epicenter. The total seismic moment was $2.3 \times 10^{21}$ Nm ($M_w$ 8.2). The synthetic waveforms calculated for this source model recovered reasonably good observations (Fig. 4.4). Figure 4.5 illustrates snapshots of the slip distribution every 5 s after rupture initiation. We can see that no large slips occurred in the first 15 s. At 20–35 s, the rupture propagated through the deep portion and toward the shallow portion of the fault plane, generating large slips. Although the shallow rupture weakened at 35–50 s, the deep rupture efficiently propagated eastward and grew to the shallow, large slip at the eastern portion of the fault plane (55–70 s). The snapshots and the moment rate function (Fig. 4.6) show that the total rupture duration was ~75 s.

To evaluate the influence of the abrupt lateral variation in the final model of Chapter 2, we

also estimated the source model by using 3-D Green's functions calculated for the smoothed final model of Chapter 2. This source model (Fig. 4.7) also yielded a seismic moment of $2.3 \times 10^{21}$ Nm ($M_w$ 8.2) and a maximum slip of ~5 m. Because direct waves show little sensitivity to the abrupt lateral variation in the final model of Chapter 2 (e.g., Fig. 2.38), there is little difference between the slip distribution of Figure 4.3 and that of Figure 4.7. In other words, such abrupt lateral variation does not deleteriously affect the result of the source inversion.

## 4.4 Discussion

### 4.4.1 Effects of the accretionary wedge on source inversions

As discussed in Chapter 3, the accretionary wedge has the effect of reducing the amplitude of ground motions in the land area. Therefore, the amplitudes of direct waves in the 3-D Green's functions are small (Fig. 3.5). This suggests that compared with the analyses using 3-D Green's functions without the accretionary wedge or 1-D Green's functions, larger slips are required to explain the observations. Figure 4.8 illustrates the slip distribution estimated by using 3-D Green's functions without the accretionary wedge. This source model yielded a seismic moment of $2.2 \times 10^{21}$ Nm ($M_w$ 8.2) and a maximum slip of ~4 m, which were slightly smaller than those for the source model with the accretionary wedge. This source model could not clearly resolve the large-slip areas seen in the source model with the accretionary wedge. Moreover, the seismic moments and the maximum slips estimated using 1-D Green's functions (Ichinose *et al.*, 2003; Yamanaka, 2004) were also smaller than our source model with the accretionary wedge, i.e., $1.2 \times 10^{21}$ Nm ($M_w$ 8.0) and ~2 m for Ichinose *et al.* (2003) and $1.5 \times 10^{21}$ Nm ($M_w$ 8.1) and ~4 m for Yamanaka (2004).

As mentioned in Section 4.1, Ichinose *et al.* (2003) and Yamanaka (2004) showed that no large slips occurred in the shallow area of the western portion of the fault plane (Fig. 4.9). On the other hand, our source model with the accretionary wedge has revealed a large slip in this

area, thus supporting previous studies that used tsunami waveform and geodetic data. Although the precise location of this shallow slip agrees well with the result of Baba *et al.* (2006), who estimated a high-precision slip distribution using tsunami waveform data, that of the deep slip near the Shima Peninsula is somewhat different from the result of Baba *et al.* (2006). The two shallow slips at the western and eastern portions of the fault plane also correspond to two large slip deficits in the Tonankai region, as observed by seafloor geodetic observations (Yokota *et al.*, 2016). Therefore, we suggest that if 1-D Green's functions without the effects of the accretionary wedge are used for source inversions for subduction earthquakes along the Nankai Trough, slip distributions cannot be appropriately estimated. Because of the existence of these two shallow slips, the duration of ground motions at the land area can be prolonged by significant surface waves (Fig. 3.5). The long durations of ground motions observed in the Kanto basin (Furumura and Nakamura, 2006; Furumura *et al.*, 2008) may be explained by these shallow slips.

### 4.4.2 Slip distribution and crustal structures

Our source model showed that the shallow slip in the western portion of the fault plane extended close to the trough axis, where a slip of ~3 m was estimated. In this area, seismic reflection profiles (Park *et al.*, 2002) found splay faults branching upward from the plate boundary. Submarine core records (Sakuguchi *et al.*, 2011) also found evidence that a slip occurred on at least the splay fault during the 1944 Tonankai earthquake. Although our fault plane did not include any branching, the slip extension to the trough axis means that the slip may have occurred on the splay fault. Because inversions based only on onshore observations cannot distinguish among plate-boundary slip, splay-fault slip, and slip partitioning (e.g., Baba *et al.*, 2006, Sakuguchi *et al.*, 2011), source inversions using both onshore and offshore observations are required for future subduction earthquakes along the Nankai Trough. To perform such source inversions, more detailed velocity structure models in the offshore area are essential and the effects of the accretionary wedge on offshore ground motions should be

appropriately evaluated.

Nakanishi *et al.* (2002b) found a particularly irregular oceanic crust around latitude 33.7–33.9°N and longitude 137.1–137.3°E, and they regarded it as a subducting seamount. This seamount is located in the area between two shallow slips at the western and eastern portions of our fault plane. Our source model has shown that the rupture propagated avoiding the seamount (35–50 s in Fig. 4.5), and the total slip around it was small (Fig. 4.3). Therefore, we suggest that the segmentation of large-slip areas is related to the existence of a seamount; in other words, the seamount itself cannot produce a large slip. Such segmentation was also reported for the 1946 Nankai earthquake (e.g., Kodaira *et al.*, 2000; Murotani *et al.*, 2015). Moreover, recent seafloor geodetic observations (Yokota *et al.*, 2016), which have better resolving power than conventional onshore observations (e.g., Loveless and Meade, 2010), provided a detailed distribution of the slip deficit along the Nankai Trough and detected the segmentations associated with seamounts.

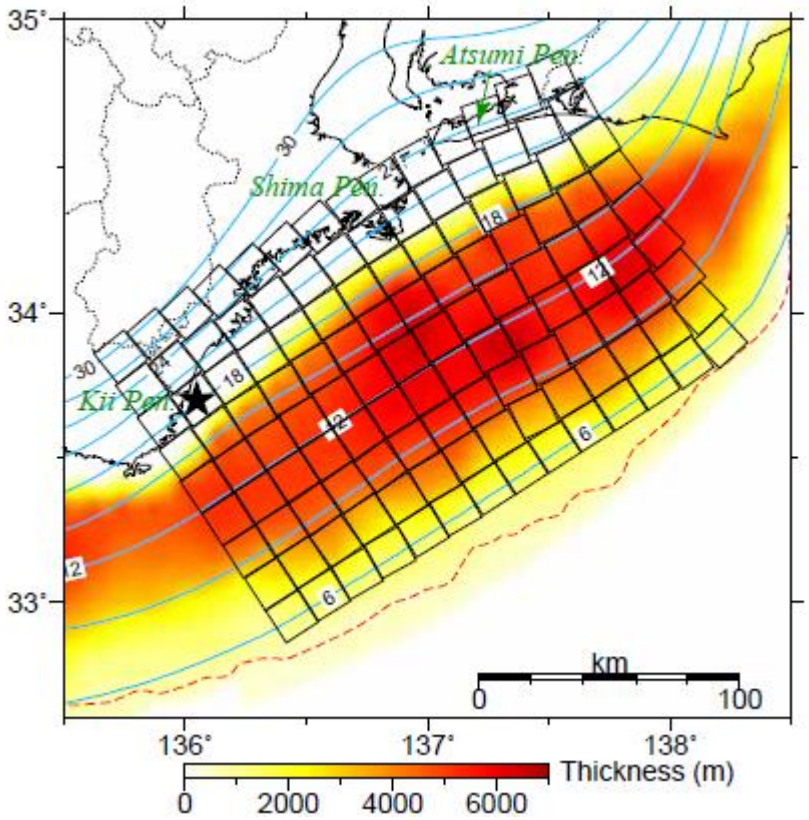


Figure 4.1 Fault plane (black grids) of the 1944 Tonankai earthquake. The background color represents the total thickness of the accretionary wedge. Contours mark the depth distribution of the top of the Philippine Sea plate. Solid star marks the epicenter.

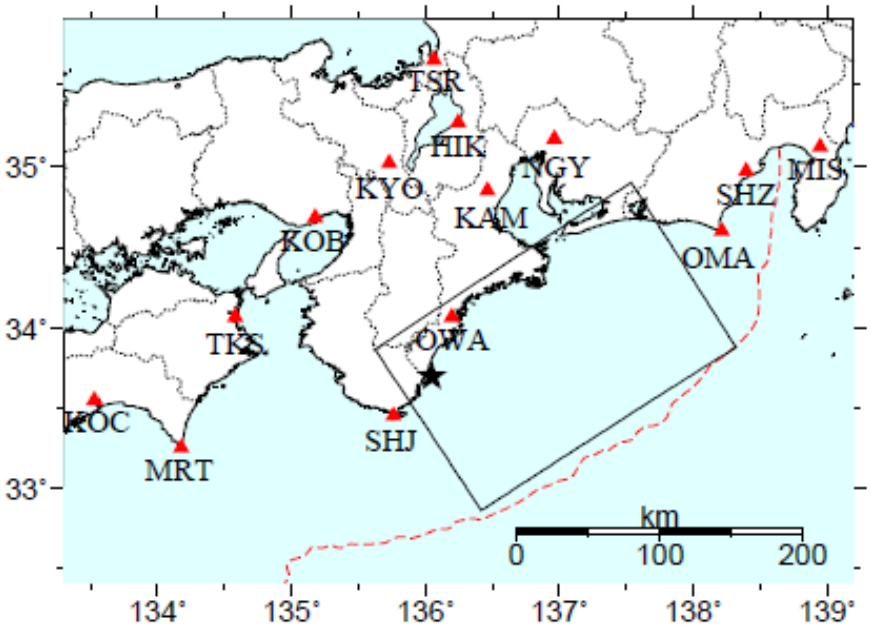


Figure 4.2 Epicenter (star), fault plane (rectangular area), and strong-motion stations (triangles) of the 1944 Tonankai earthquake.

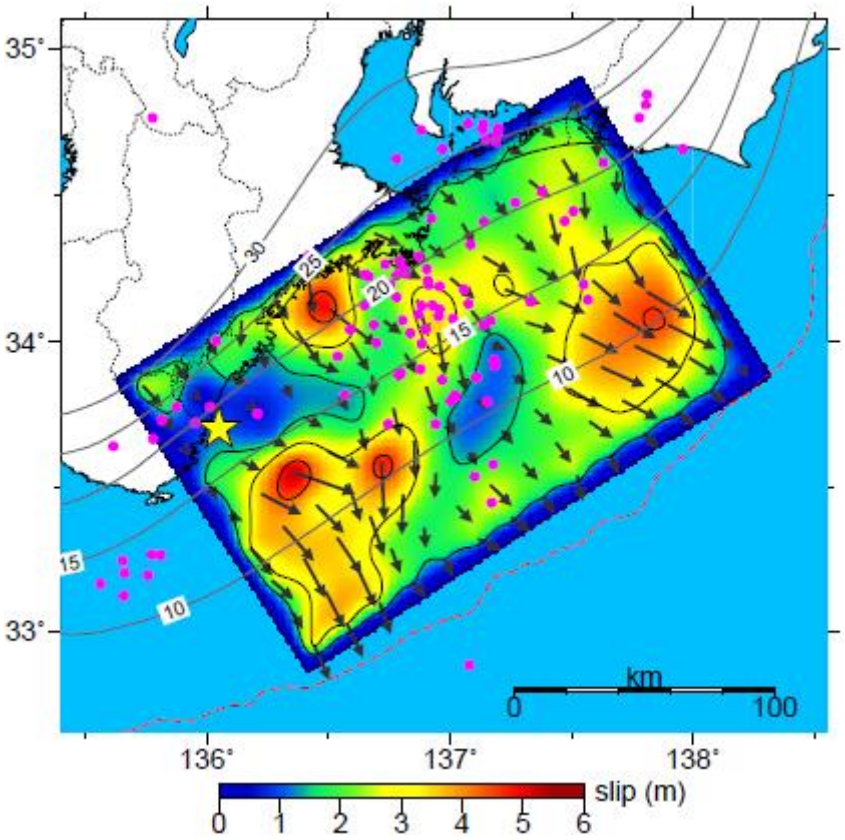


Figure 4.3 Slip distribution of the 1944 Tonankai earthquake (estimated using the final model of Chapter 2). Arrows indicate subfault slips on the hanging wall. Purple circles denote epicenters of the aftershocks until January 11, 1945 (JST).

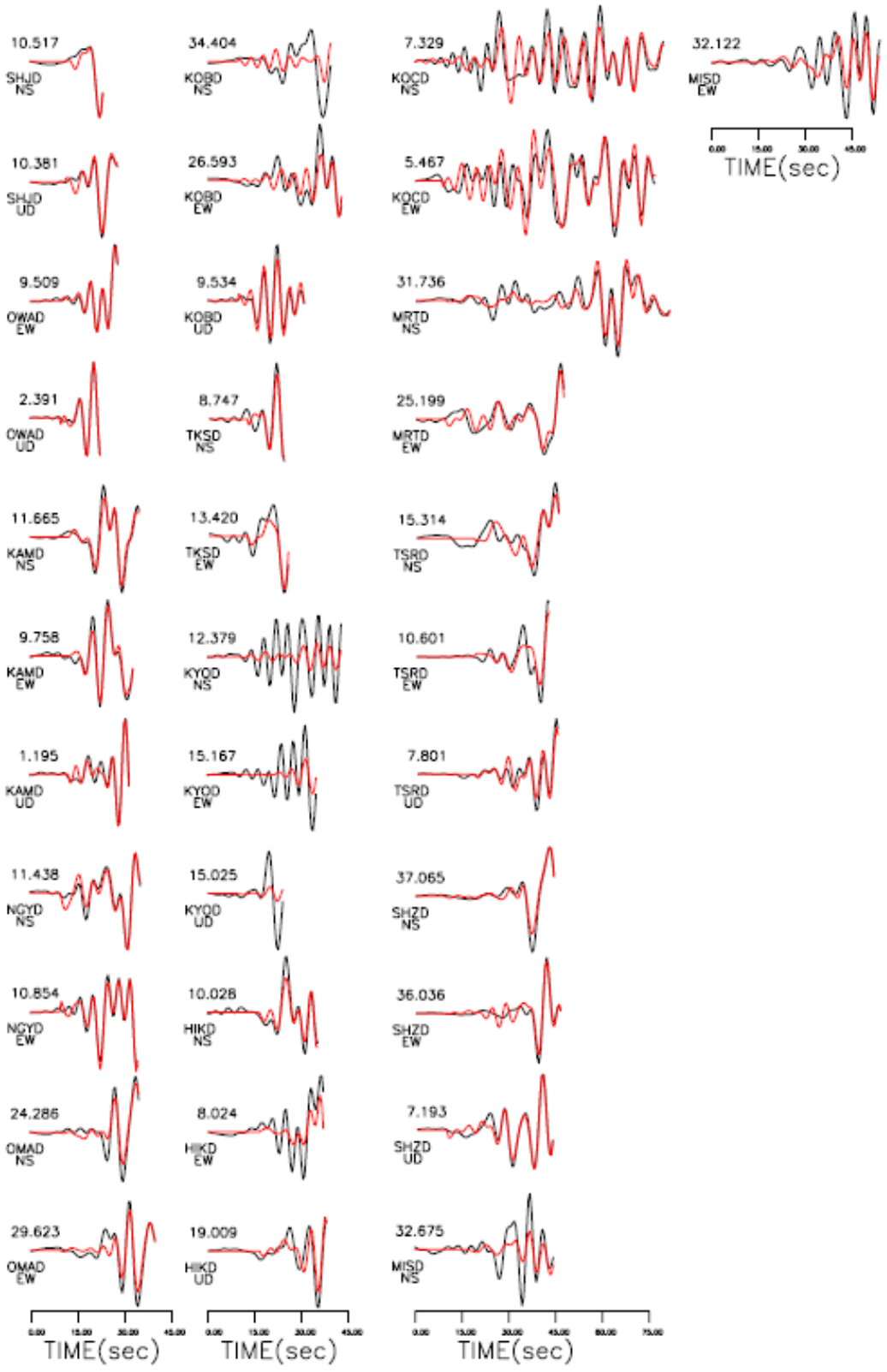


Figure 4.4 Comparison between the observed (black) and synthetic (red) waveforms. The numbers on the left side of waveforms are the peak amplitudes of the observed waveforms (unit: cm). Note that all waveforms include instrumental responses of seismographs.

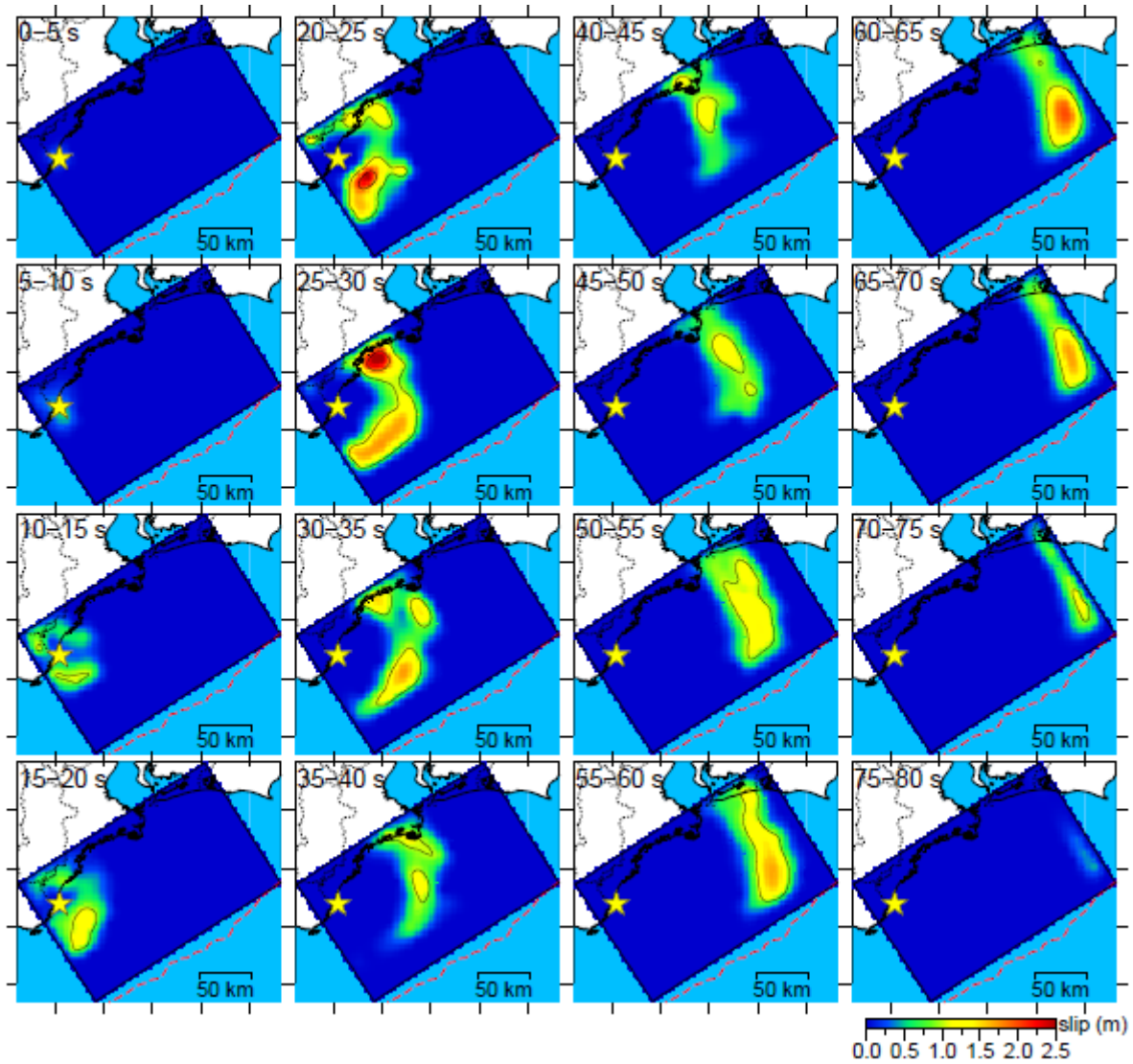


Figure 4.5 Snapshots of the slip distribution every 5 s.

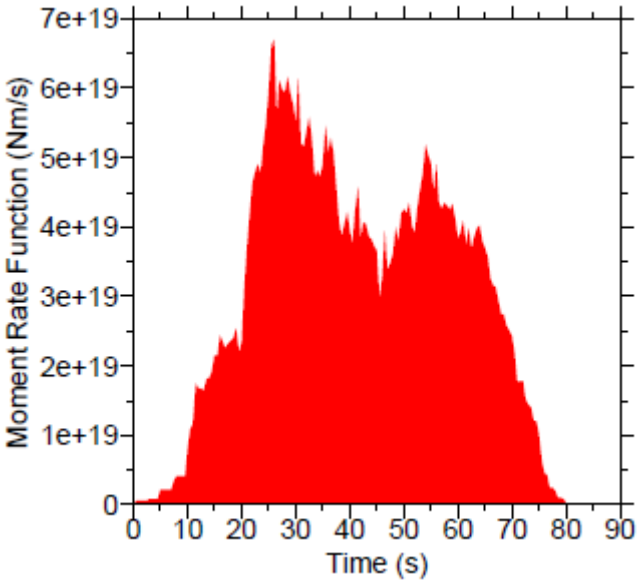


Figure 4.6 Final moment rate function.

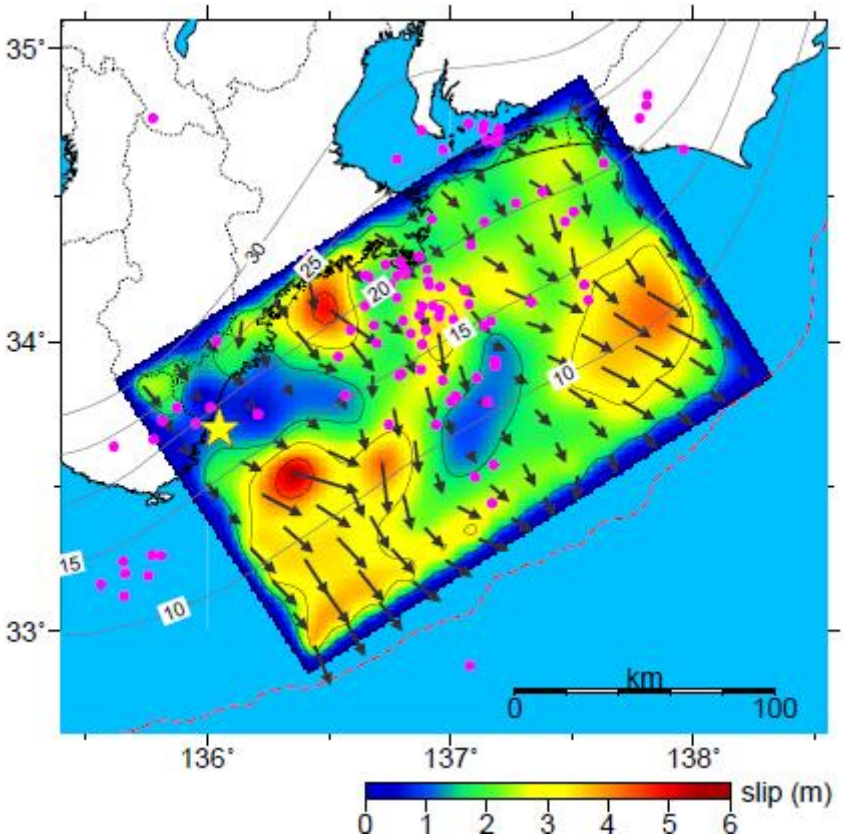


Figure 4.7　Slip distribution of the 1944 Tonankai earthquake estimated using the smoothed final model of Chapter 2. Arrows indicate subfault slips on the hanging wall. Purple circles denote epicenters of the aftershocks until January 11, 1945 (JST).

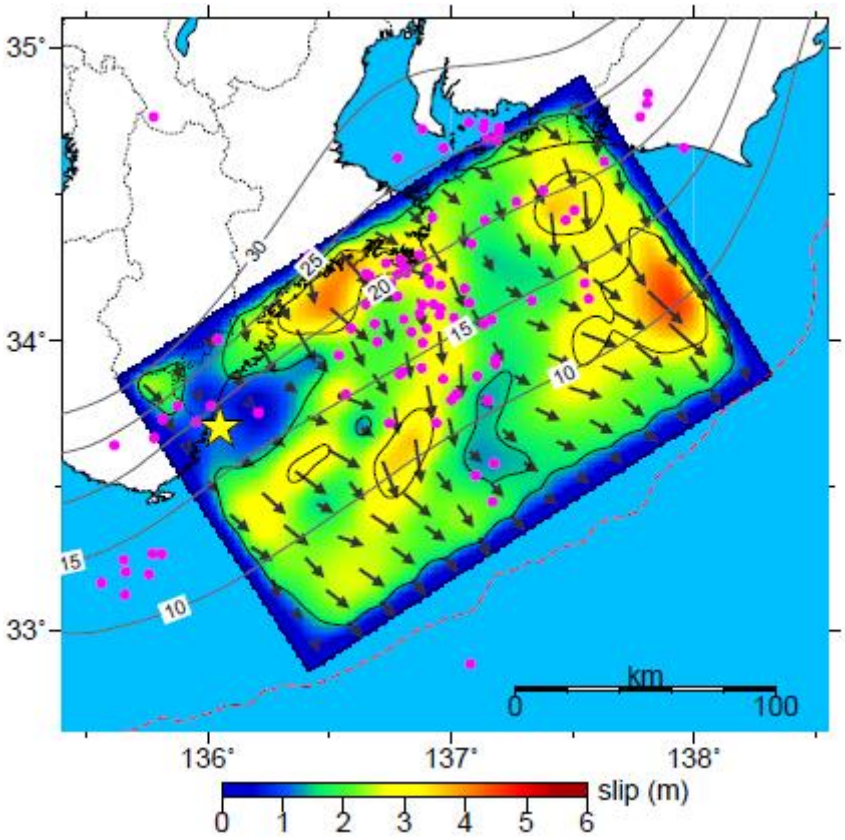


Figure 4.8 Slip distribution in the case of 3-D Green's functions without the accretionary wedge.

Figure 4.9　Inversion results of Ichinose *et al.* (2003) and Yamanaka (2004).

図 4.9

インターネット公表に対する著作権者からの許諾が得られていないため、非公開。

# Chapter 5
# Conclusions

We have proposed a full-waveform inversion method for 3-D velocity structures. In this inversion, the thicknesses of the layers in the velocity structures are model parameters; thus, the 3-D geometries of the layer boundaries are estimated. The partial derivatives with respect to model parameters are calculated by a finite-difference approximation. Our inversion introduced an efficient approach, termed the multiscale approach, in which the inverted frequency band is expanded from low frequency to high frequency. The multiscale approach is effective in overcoming local minima in the inversion problem and is suitable for cases in which the initial model is far from the solution. Moreover, the multiscale approach has the advantage of significantly reducing the total number of 3-D forward simulations for calculating partial derivatives with respect to model parameters. By performing synthetic tests, we have confirmed the validity of the multiscale waveform inversion.

Subsequently, we have applied the multiscale waveform inversion to real data to estimate 3-D velocity structures of the accretionary wedge in the Tonankai region. The waveforms (0.08–0.25 Hz) recorded at both onshore and offshore stations during a 6.0 $M_w$ earthquake were used for the inversion. We have used a 3-D velocity structure model of the accretionary wedge, which was compiled based on several seismic surveys, as the initial model. We have performed the inversion from 0.08–0.125 to 0.08–0.25 Hz. When updated by the inversion, the velocity structure model of the accretionary wedge had thicker low-velocity layers and was richer in lateral variation than the initial model. We have performed several validation tests and concluded that the updated model was better than the initial model in terms of reproducing observed ground motions.

Next, we have deployed numerous virtual point sources to cover the plate boundary in the Tonankai region and performed 3-D ground motion simulations to evaluate the effects of the

accretionary wedge on ground motions in the land area. The updated velocity structure model of the accretionary wedge has been used for the simulations. The simulation results have shown that the accretionary wedge has the effect of decreasing the peak amplitude and elongating the duration of ground motions. The duration of ground motions for shallow sources with a depth of less than ~10 km is significantly long because of the existence of large basin-induced surface waves excited at the boundary between the accretionary wedge and the crust near the trough axis. We have also found that the amplitude reduction is restricted to periods of less than ~10 s. This finding can explain the predominant period of ground motions observed in the land area. Moreover, owing to the coupling effect between the accretionary wedge and ocean water, the amplitude reduction of fundamental-mode Rayleigh waves caused by seawater occurs at periods longer than those in the case of the absence of the accretionary wedge. We suggest that ground motions in the land area are dominated by higher-mode surface waves because fundamental-mode surface waves are significantly trapped by the accretionary wedge and seawater.

Finally, we have estimated the rupture process of the 1944 Tonankai earthquake by the inversion of strong-motion data, for which 3-D Green's functions were calculated. The seismic moment and maximum slip were estimated to be $2.3 \times 10^{21}$ Nm ($M_w$ 8.2) and ~5 m, respectively, which were larger than the results of the 1-D Green's functions and 3-D Green's functions without the accretionary wedge. The estimated large-slip areas are consistent with the large slip deficits observed by seafloor geodetic observations. We suggest that owing to the de-amplification effect of the accretionary wedge on ground motions at the land area, source inversions using 1-D Green's functions or 3-D Green's functions that do not consider this effect can result in underestimations of the seismic moment and the maximum slip.

The multiscale waveform inversion for 3-D velocity structures proposed by this study is also applicable to other regions such as sedimentary basins in the land area. Since the multiscale waveform inversion can reduce 3-D computational costs, we believe that it will be widely used to improve 3-D velocity structure models. Because no ocean-bottom observation

networks were available in the Nankai and Tokai regions in 2016, we have improved the velocity structure model of the accretionary wedge only in the Tonankai region. Future observation networks in the Nankai and Tokai regions will enable the improvement of 3-D velocity structure models and allow for a better understanding of the effects of the accretionary wedge, following the approach presented here.

The details of the effects of an accretionary wedge depend on its 3-D velocity structures and thus have regional dependence. However, accretionary wedges along other subduction zones are likely to show effects that are qualitatively similar to those observed for the Tonankai region because they also have 3-D sedimentary structures with low velocities. In particular, the effects seen for propagation mechanisms suggested by this study, such as basin-induced surface waves and frequency dependencies, may provide valuable insights into the effects of accretionary wedges along other subduction zones.

# References


Anderson, J. G., P. Bodin, J. N. Brune, J. Prince, S. K. Singh, R. Quaas, and M. Onate (1986). Strong ground motion from the Michoacan, Mexico, earthquake, *Science* **233,** 1043-1049.

Aoi, S. (2002). Bondary shape waveform inversion for estimating the depth of three-dimensional basin structures, *Bull. Seismol. Soc. Am.* **92,** 2410–2418.

Aoi, S., T. Kunugi, H. Nakamura, and H. Fujiwara (2011). Deployment of new strong motion seismographs of K-NET and KiK-net, in *Earthquake Data in Engineering Seismology*, Geotechnical, Geological, and Earthquake Engineering, Vol. 14, Springer, Dordrecht, The Netherlands, 167–186.

Aoi, S., R. Honda, N. Morikawa, H. Sekiguchi, H. Suzuki, Y. Hayakawa, T. Kunugi, and H. Fujiwara (2008). Three-dimensional finite difference simulation of long-period ground motions for the 2003 Tokachi-oki, Japan, earthquake, *J. Geophys. Res.* **113,** no. B07302, doi: 10.1029/2007JB005452.

Askan, A., and J. Bielak (2008). Full anelastic waveform tomography including model uncertainty, *Bull. Seismol. Soc. Am.* **98,** 2975–2989, doi: 10.1785/0120080138.

Baba, T., and P. R. Cummins (2005). Contiguous rupture areas of two Nankai Trough earthquakes revealed by high-resolution tsunami waveform inversion, *Geophys. Res. Lett.* **32,** L08305, doi:10.1029/2004GL022320.

Baba, T., P. R., Cummins, T. Hori, and Y. Kaneda (2006). High precision slip distribution of the 1944 Tonankai earthquake inferred from tsunami waveforms: Possible slip on a splay fault, *Tectonophysics*, **426,** 119–134.

Bard, P.-Y., and M. Bouchon (1980a). The seismic response of sediment-filled valleys. Part 1. The case of incident *SH* waves, *Bull. Seismol. Soc. Am.* **70,** 1263–1286.

Bard, P.-Y., and M. Bouchon (1980b). The seismic response of sediment-filled valleys. Part 2.

The case of incident *P* and *SV* waves, *Bull. Seismol. Soc. Am.* **70,** 1921–1941.

Beck, J. L., and J. F. Hall (1986). Factors contributing to the catastrophe in Mexico City during the earthquake of September 19, 1985, *Geophys. Res. Lett.* **13,** 593–596.

Bowden, D. C., M. D. Kohler, V. C. Tsai, and D. S. Weeraratne (2016). Offshore Southern California lithospheric velocity structure from noise cross-correlation functions, *J. Geophys. Res. Solid Earth* **121,** 3415–3427, doi: 10.1002/2016JB012919.

Bradley, B. A. (2012). Strong ground motion characteristics observed in the 4 September 2010 Darfield, New Zealand earthquake, *Soil Dynamics and Earthquake Engineering*, **2012,** 32–46.

Bunks, C., F. M. Saleck, S. Zaleski, and G. Chavent (1995). Multiscale seismic waveform inversion, *Geophysics* **60,** 1457–1473.

Chen, P., L. Zhao, and T. H. Jordan (2007). Full 3D tomography for the crustal structure of the Los Angeles region, *Bull. Seismol. Soc. Am.* **97,** 1094–1120, doi: 10.1785/0120060222.

Chen, H., J.-M. Chiu, J. Pujol, K. Kim, K.-C. Chen, B.-S. Huang, Y.-H., Yeh, and S.-C., Chiu (2006). A simple algorithm for local earthquake location using 3D $V_P$ and $V_S$ models: Test examples in the central United States and central eastern Taiwan, *Bull. Seismol. Soc. Am.* **96,** 288–305, doi: 10.1785/0120040102.

Ekstrom, G., M. Nettles, and A. M. Dziewonki (2012). The global CMT project 2004–2010: Centroid-moment tensors for 13,017 earthquakes, *Phys. Earth Planet. Inter.* **200**–**201,** 1–9.

Ewing, W. M., W. S. Jardetzky, and F. Press (1957). *Elastic Waves in Layered Media*, McGraw Hill Book Company, Inc., New York, America, 405pp.

Expedition 314 Scientists (2009). Expedition 314 Site C0002, in *Proc. IODP*, Vol. 314/315/316, Integrated Ocean Drilling Program Management International, Inc., Washington, D.C., America, 77pp.

Fujiwara, H., S. Kawai, S. Aoi, N. Morikawa, S. Senna, N. Kudo, M. Ooi, K. X.-S. Hao, Y.

Hayakawa, N. Toyama, H. Matsuyama, K. Iwamoto, H. Suzuki, and Y. Liu (2009). A study on subsurface structure model for deep sedimentary layers of Japan for strongmotion evaluation, Technical Note of the National Research Institute for Earth Science and Disaster Prevention 337 (in Japanese).

Fujiwara, H., S. Kawai, S. Aoi, N. Morikawa, S. Senna, H. Azuma, M. Ooi, K. X.-S. Hao, N. Hasegawa, T. Maeda, A. Iwaki, K. Wakamatsu, M. Imoto, T. Okumura, H. Matsuyama, and A. Narita (2012). Some improvements of seismic hazard assessment based on the 2011 Tohoku earthquake, *Technical Note of the National Research Institute for Earth Science and Disaster Prevention* 379 (in Japanese).

Furumura, T., and K. Koketsu (1998). Specific distribution of ground motion during the 1995 Kobe earthquake and its generation mechanism, *Geophys. Res. Lett.* **25,** 785–788.

Furumura, T., and M. Nakamura (2006). Recovering of strong motion record of the 1944 Tonankai earthquake and long period ground motion in Kanto region, *Butsuri-Tansa*, **59,** 337–351 (in Japanese with English abstract).

Furumura, T., and S. K. Singh (2002). Regional wave propagation from Mexican subduction zone earthquakes: the attenuation functions for interplate and inslab events, *Bull. Seismol. Soc. Am.* **92,** 2110–2125.

Furumura, T., T. Hayakawa, M. Nakamura, K. Koketsu, and T. Baba (2008). Development of long-period ground motions from the Nankai Trough, Japan, earthquakes: Observations and computer simulation of the 1944 Tonankai ($M_w$ 8.1) and the 2004 SE off-Kii Peninsula ($M_w$ 7.4) earthquakes, *Pure Appl. Geophys.* **165,** 585–607.

Goto. K., and M. Nagano (2015). Influence of velocity structure around the Philippine Sea plate on long-period ground motion evaluation in Osaka plain, *J. Technol. Des. AIJ* **21,** 955–960 (in Japanese with English abstract).

Graves, R. W., and D. J. Wald (2001). Resolution analysis of finite fault source inversion using one- and three-dimensional Green's functions 1. Strong motions, *J. Geophys. Res.* **106,** 8745–8766.

Graves, R. W., and D. J. Wald (2004). Observed and simulated ground motions in the San Bernardino basin region for the Hector Mine, California, earthquake, *Bull. Seismol. Soc. Am.* **94,** 131–146.

Guo, Y., K. Koketsu, and T. Ohno (2013). Analysis of the rupture process of the 1995 Kobe earthquake using a 3D velocity structure, *Earth Planets Space* **65,** 1581–1586.

Guo, Y., K. Koketsu, and H. Miyake (2016). Propagation mechanism of long-period ground motions for offshore earthquakes along the Nankai Trough: Effects of the accretionary wedge, *Bull. Seismol. Soc. Am.* **106,** 1176–1197, doi: 10.1785/0120150315.

Gualtieri, L., E. Stutzmann, Y. Capdeville, V. Farra, A. Mangeney, and A. Morelli (2015). On the shaping factors of the secondary microseismic wavefield, *J. Geophys. Res. Solid Earth* **120,** 6241–6262, doi: 10.1002/2015JB012157.

Gvirtzman, Z., and J. N. Louie (2010). 2D analysis of earthquake ground motions in Haifa Bay, Israel, *Bull. Seismol. Soc. Am.* **100,** 733–750, doi: 10.1785/0120090019.

Haberland, C., A. Rietbrock, D. Lange, K. Bataille, and T. Dahm (2009). Structure of the seismogenic zone of the southcentral Chilean margin revealed by local earthquake traveltime tomography, *J. Geophys. Res.* **114,** no. B01317, doi: 10.1029/2008JB005802.

Harmon, N., T. Henstock, F. Tilmann, A. Rietbrock, and P. Barton (2012). Shear velocity structure across the Samatran Forearc-Arc, *Geophys. J. Int.* **189,** 1306–1314, doi: 10.1111/j.1365–246X.2012.05446.x.

Hatayama, K. (2004). Theoretical evaluation of effects of sea on seismic ground motion, *Proc. of the 13th World Conf. on Earthq. Eng.*, Vancouver, D.C., Canada, 1–6 August 2004, Paper No. 3229.

Hayashimoto, N., and M. Hoshiba (2013). Examination of travel time correction and magnitude correction of Tonankai ocean bottom seismographs for earthquake early warning, *Quart. J. Seismol.* **76,** 69–81 (in Japanese with English abstract).

Hayashimoto, N., and M. Hoshiba (2015). Installation azimuth of Tonankai OBS estimated from air-gun data, *Quart. J. Seismol.* **78,** 159–167 (in Japanese with English abstract).

Headquarters for Earthquake Research Promotion (2013). Evaluations of occurrence potentials or subduction-zone earthquakes, http://www.jishin.go.jp/main/chousa/13may_nankai/index.htm (last accessed December 2016) (in Japanese).

Hikima, K. (2006). Waveform inversion for 3-D velocity structures and source process analyses using its results, *PhD thesis*, Department of Earth and Planetary Science, The University of Tokyo, Japan, 171pp (in Japanese with English abstract).

Hikima, K., and K. Koketsu (2005). Rupture processes of the 2004 Chuetsu (mid-Niigata prefecture) earthquake, Japan: A series of events in a complex fault system, *Geophys. Res. Lett.* **32,** L18303, doi: 1029/2005GL023588.

Ichinose, G. A., H. K. Thio, and P. G. Somerville (2003). Rupture process of the 1944 Tonankai earthquake ($M_s$ 8.1) from the inversion of teleseismic and regional seismograms, *J. Geophys. Res.* **108,** no. B10, 2497, doi: 10.1029/2003JB002393.

Ikegami, Y., K. Koketsu, T. Kimura, and H.Miyake (2008). Finite-element simulations of long-period ground motions: Japanese subduction-zone earthquakes and the 1906 San Francisco earthquake, *J. Seismol.* **12,** 161–172, doi: 10.1007/s10950–008–9091–5.

Iwaki, A., and T. Iwata (2010). Simulation of long-period ground motion in the Osaka sedimentary basin: Performance estimation and the basin structure effects, *Geophys. J. Int.* **181,** 1062–1076, doi: 10.1111/j.1365–246X.2010.04556.x.

Iwaki, A., and T. Iwata (2011). Estimation of three-dimensional boundary shape of the Osaka sedimentary basin by waveform inversion, *Geophys. J. Int.* **186,** 1255–1278, doi: 10.1111/j.1365–246X.2011.05102.x.

Kagawa, T., A. Petukhin, K. Koketsu, H. Miyake, and S. Murotani (2012). Source modeling for long-period ground motion simulation of the 1946 Nankai earthquake, Japan, *Proc. of the 15th World Conf. on Earthq. Eng.*, Lisbon, Portugal, 24–28 September 2012, Paper No. 0806.

Kamei, R., R. G. Pratt, and T. Tsuji (2012). Waveform tomography imaging of a megasplay

fault system in the seismogenic Nankai subduction zone, *Earth Planet. Sci. Lett.* **317/318,** 343–353.

Kanamori, H. (1972) Tectonic implications of the 1944 Tonankai and the 1946 Nankaido earthquakes, *Phys. Earth Planet. Inter.*, **5,** 129–139.

Kaneda, Y., K. Kawaguchi, E. Araki, H. Matsumoto, T. Nakamura, S. Kamiya, K. Ariyoshi, T. Hori, T. Baba N. Takahashi (2015). Development and application of an advanced ocean floor network system for megathrust earthquakes and tsunamis, in *Seafloor Observatories: A New Vision of the Earth from the Abyss*, Springer, Dordrecht, The Netherlands, 643–662.

Kato, T., and M, Ando (1997). Source mechanisms of the 1944 Tonankai and 1946 Nankaido earthquakes: Spatial heterogeneity of rise times, *Geophys. Res. Lett.* **24**, 2055–2058.

Kawabe, H., and K. Kamae (2008). Prediction of long-period ground motions from huge subduction earthquakes in Osaka, Japan, *J. Seismol.* **12,** 173–184, doi: 10.1007/s10950–008–9089–z.

Kawase, H. (2003). Site effects on strong ground motions, in *International Handbook of Earthquake and Engineering Seismology, Part B*, W. H. K. Lee, H. Kanamori, P. C. Jennings, and C. Kisslinger (Editors), Academic Press, New York, America, 1013–1030.

Kobayashi, R., and E. Araki (2016). Source process of the 2016 southeast off Mie Prefecture earthquake, *2016 SSJ Fall Meeting*, Nagoya, Japan, 5–7 October 2016, Abstract S08–P01 (in Japanese).

Kodaira, S., N. Takahashi, A. Nakanishi, S. Miura, and Y. Kaneda (2000). Subducted seamount imaged in the rupture zone of the 1946 Nankaido earthquake, *Science*, **289,** 104–106.

Koketsu, K. (1989) Hypocenter determination with non-negative depth, *Zisin* **42,** 325–331 (in Japanese with English abstract).

Koketsu, K., and M. Kikuchi (2000). Propagation of seismic ground motion in the Kanto basin, Japan, *Science* **288,** 1237–1239.

Koketsu, K., H. Fujiwara, and Y. Ikegami (2004). Finite-element simulation of seismic ground motion with a voxel mesh, *Pure Appl. Geophys.* **161,** 2183–2198.

Koketsu, K., H. Miyake, and H. Suzuki (2012). Japan Integrated Velocity Structure Model Version 1, *Proc. of the 15th World Conf. on Earthq. Eng.*, Lisbon, Portugal, 24–28 September 2012, Paper No. 1773.

Koketsu, K., H. Miyake, Afnimar, and Y. Tanaka (2009). A proposal for a standard procedure of modeling 3-D velocity structures and its application to the Tokyo metropolitan area, Japan, *Tectonophysics* **472,** 290–300.

Koketsu, K., H. Miyake, H. Fujiwara, and T. Hashimoto (2008). Progress towards a Japan integrated velocity structure model and long-period ground motion hazard map, *Proc. of the 14th World Conf. on Earthq. Eng.*, Beijing, China, 12–17 October 2008, Paper No. S10–038.

Lee, E.-J., P. Chen, T. H. Jordan, P. B. Maechling, M. A. M. Denolle, and G. C. Beroza (2014). Full-3-D tomography for crustal structure in Southern California based on the scattering-integral and the adjoint-wavefield methods, *J. Geophys. Res. Solid Earth* **119,** 6421–6451, doi: 10.1002/2014JB011346.

Liu, P., and R. J. Archuleta (2004). A new nonlinear finite fault inversion with three-dimensional Green's functions: Application to the 1989 Loma Prieta, California, earthquake, *J. Geophys. Res.* **109,** no. B02318, doi:10.1029/2003JB002625.

Loveless, J. P., and B. J. Meade (2010). Geodetic imaging of plate motions, slip rates, and partitioning of deformation in Japan, *J. Geophys. Res.* **115,** no. B02410, doi: 10.1029/2008JB006248.

Maeda, T., T. Furumura, and K. Obara (2014). Scattering of teleseismic *P*-waves by the Japan Trench: A significant effect of reverberation in the seawater column, *Earth Planet. Sci. Lett.* **397,** 101–110.

Maeda, T., K. Obara, T. Furumura, and T. Saito (2011). Interference of long-period seismic wavefield observed by the dense Hi-net array in Japan, *J. Geophys. Res.* **116,** no.

B10303, doi: 10.1029/2011JB008464.

Maeda, T., T. Furumura, S. Noguchi, S. Takemura, S. Sakai, M. Shinohara, K. Iwai, and S. J. Lee (2013). Seismic and tsunami wave propagation of the 2011 Off the Pacific Coast of Tohoku Earthquake as inferred from the tsunami-coupled finite difference simulation, *Bull. Seismol. Soc. Am.* **103,** 1456–1472, doi: 10.1785/0120120118.

Menke, W. (1989). *Geophysical Data Analysis: Discrete Inversion Theory (Revised Edition)*, Academic Press, San Diego, America, 289pp.

Miyakoshi, K., and M. Horike (2006). Predominant period of the long-period ground motions in the Osaka basin, *Butsuri-Tansa*, **59,** 327–336 (in Japanese with English abstract).

Mochizuki, K., G. Fujie, T. Sato, and J. Kasahara (1998). Heterogeneous crustal structure across a seismic block boundary along the Nankai Trough, *Geophys. Res. Lett.* **25,** 2301–2304.

Murotani, S., K. Shimazaki, and K. Koketsu (2015). Rupture process of the 1946 Nankai earthquake estimated using seismic waveforms and geodetic data, *J. Geophys. Res. Solid Earth* **120,** 5677–5692, doi: 10.1002/2014JB011676.

Nakamura, T., H. Takenaka, T. Okamoto, and Y. Kaneda (2012). FDM Simulation of seismic-wave propagation for an aftershock of the 2009 Suruga Bay earthquake: Effects of ocean-bottom topography and seawater Layer, *Bull. Seismol. Soc. Am.* **102,** 2420–2435, doi: 10.1785/0120110356.

Nakamura, T., H. Takenaka, T. Okamoto, and Y. Kaneda (2014b). Seismic wavefields in the deep seafloor area from a submarine landslide source, *Pure Appl. Geophys.* **171,** 1153–1167.

Nakamura, T., H. Takenaka, T. Okamoto, M. Ohori, and S. Tsuboi (2015). Long-period ocean-bottom motions in the source areas of large subduction earthquakes, *Sci. Rep.* **5,** no. 16648, doi: 10.1038/srep16648.

Nakamura, T., M. Nakano, N. Hayashimoto, N. Takahashi, H. Takenaka, T. Okamoto, E. Araki, and Y. Kaneda (2014a). Anomalously large seismic amplifications in the seafloor

area off the Kii peninsula, *Mar. Geophys. Res.* **35,** 255–270, doi: 10.1007/s11001–014–9211–2.

Nakanishi, I. (1992). Rayleigh waves guided by sea-trench topography, *Geophys. Res. Lett.* **12,** 2385–2388.

Nakanishi, A., H. Shiobara, R. Hino, J. Kasahara, K. Suyehiro, and H. Shimamura (2002b). Crustal structure around the eastern end of coseismic rupture zone of the 1944 Tonankai earthquake, *Tectonophysics*, **354,** 257–275.

Nakanishi, A., H. Shiobara, R. Hino, S. Kodaira, T. Kanazawa, and H. Shimamura (1998). Detailed subduction structure across the eastern Nankai Trough obtained from ocean bottom seismographic profiles, *J. Geophys. Res.* **103,** no. B11, 27,151–27,168.

Nakanishi, A., N. Takahashi, J.-O. Park, S. Miura, S. Kodaira, Y. Kaneda, N. Hirata, T. Iwasaki, and M. Nakamura (2002a). Crustal structure across the coseismic rupture zone of the 1944 Tonankai earthquake, the central Nankai Trough seismogenic zone, *J. Geophys. Res.* **107,** no. B1, EPM 2–1–EPM 2–21, doi: 10.1029/2001JB000424.

Nakano, M., T. Nakamura, and Y. Kaneda (2015). Hypocenters in the Nankai Trough determined by using data from both ocean-bottom and land seismic networks and a 3D velocity structure model: Implications for seismotectonic activity, *Bull. Seismol. Soc. Am.* **105,** 1594–1605, doi: 10.1785/0120140309.

Nishida, K., H. Kawakatsu, and K. Obara (2008). Three-dimensional crustal *S* wave velocity structure in Japan using microseismic data recorded by Hi-net tiltmeters, *J. Geophys. Res.* **113,** no. B10302, doi: 10.1029/2007JB005395.

Noguchi, S., T. Maeda, and T. Furumura, (2013). FDM simulation of an anomalous later phase from the Japan Trench subduction zone earthquakes, *Pure Appl. Geophys.*, **170,** 95–108.

Noguchi, S., T. Maeda, and T. Furumura, (2016). Ocean-influenced Rayleigh waves from outer-rise earthquakes and their effects on durations of long-period ground motion, *Geophys. J. Int.* **205,** 1099–1107, doi: 10.1093/gji/ggw074.

Obana, K., S. Kodaira, and Y. Kaneda (2009). Seismicity at the eastern end of the 1944 Tonankai earthquake rupture area, *Bull. Seismol. Soc. Am.* **99,** 110–122, doi: 10.1785/0120070236.

Olsen, K. B., W. J. Stephenson, and A. Geisselmeyer (2008). 3D crustal structure and long-period ground motions from a M9.0 megathrust earthquake in the Pacific Northwest region, *J. Seismol.* **12,** 145–159, doi: 10.1007/s10950–007–9082–y.

Park, J.-O., T. Tsuru, S. Kodaira, P. R. Cummins, and Y. Kaneda (2002). Splay fault branching along the Nankai subduction zone, *Science* **297,** 1157–1160.

Petukhin, A., T. Iwata, and T. Kagawa (2010). Study on the effect of the oceanic water layer on strong ground motion simulations, *Earth Planets Space* **62,** 621–630.

Petukhin, A., K. Miyakoshi, M. Tsurugi, H. Kawase, and K. Kamae (2016). Visualization of Green's function anomalies for megathrust source in Nankai trough by reciprocity method, *Earth Planets Space* **68,** no. 4, doi: 10.1186/s40623–016–0385–5.

Pitarka, A., R. G. Graves, and P. Somerville (2004). Validation of a 3D velocity model of the Puget Sound region based on modeling ground motion from the 28 February 2001 Nisqually earthquake, *Bull. Seismol. Soc. Am.* **94,** 1670–1689.

Quinay, P. E. B., T. Ichimura, and M. Hori (2012). Waveform inversion for modeling three-dimensional crust structure with topographic effects, *Bull. Seismol. Soc. Am.* **102,** 1018–1029, doi: 10.1785/0120110175.

Sagiya, T., and W. Thatcher (1999). Coseismic slip resolution along a plate boundary megathrust: The Nankai Trough, southwest Japan, *J. Geophys. Res.* **104,** 1111–1129.

Sakaguchi, A., G. Kimura, M. Strasser, E. J. Screaton, D. Curewitz, and M. Murayama (2011). Episodic seafloor mud brecciation due to great subduction zone earthquakes, *Geology*, **39,** 919–922, doi: 10.1130/G32043.1.

Saito, M. (1988). DISPER80: A subroutine package for the calculation of seismic normal-mode solutions, in *Seismological Algorithms: Computational Methods and Computer Programs*, D. J. Doornbos (Editor), Academic Press, New York, America,

293–319.

Saito, S. (2007). JMA's new Ocean Bottom Seismographs (OBS) using marine cable installed at the Sea of Enshu to the Sea of Kumano, *Chikyu Monthly* **29,** 516–522 (in Japanese).

Sarah, M. K., D. Zhao, J. Lei, and M. F. Abdelwahed (2005). Crustal heterogeneity beneath southwest Japan estimated from direct and Moho-reflected waves, *Tectnonophysics* **395,** 1–17.

Satake, K. (1993). Depth distribution of coseismic slip along the Nankai Trough, Japan, from joint inversion of geodetic and tsunami data, *J. Geophys. Res.* **98,** 4553–4565.

Shapiro, N. M., M. Campillo, S. K. Singh, and J. Pacheco (1998). Seismic channel waves in the accretionary prism of the Middle America Trench, *Geophys. Res. Lett.* **25,** 101–104.

Shapiro, N. M., K. B. Olsen, and S. K. Singh (2002). On the duration of seismic motion incident onto the Valley of Mexico for subduction zone earthquakes, *Geophys. J. Int.* **151,** 501–510.

Smith, W. H. F., and P. Wessel (1990). Gridding with continuous curvature splines in tension, *Geophysics* **55,** 293–305.

Takahashi, N., S. Kodaira, A. Nakanishi, J.-O. Park, S. Miura, T. Tsuru, Y. Kaneda, K. Suyehiro, and H. Kinoshita (2002). Seismic structure of western end of the Nankai trough seismogenic zone, *J. Geophys. Res.* **107,** no. B10, ESE 2–1–ESE 2–19, doi: 10.1029/2000JB000121.

Takekoshi, M., and H. Yamanaka (2009). Waveform inversion of shallow seismic refraction data using hybrid heuristic search method, *Exploration Geophysics*, **40,** 99–104.

Takeo, A., D. W. Forsyth, D. S. Weeraratne, and K. Nishida (2014). Estimation of azimuthal anisotropy in the NW Pacific from seismic ambient noise in seafloor records, *Geophys. J. Int.* **199,** 11–22, doi: 10.1093/gji/ggu240.

Tanioka, Y., and K. Satake (2001). Detailed coseismic slip distribution of the 1944 Tonankai earthquake estimated from tsunami waveforms, *Geophys. Res. Lett.* **28,** 1075–1078.

Tape, C., Q. Liu, and J. Tromp (2007). Finite-frequency tomography using adjoint methods−

Methodology and examples using membrane surface waves, *Geophys. J. Int.* **168,** 1105–1129, doi: 10.1111/j.1365–246X.2006.03191.x.

Tape, C., Q. Liu, A. Maggi, and J. Tromp (2010). Seismic tomography of the southern California crust based on spectral-element and adjoint methods, *Geophys. J. Int.* **180,** 433–462, doi: 10.1111/j.1365–246X.2009.04429.x.

Tobin, H., M. Kinoshita, M. K. Thu, and the Expedition 314 Scientists (2009). Expedition 314 summary, in *Proc. IODP*, Vol. 314/315/316, Integrated Ocean Drilling Program Management International, Inc., Washington, D.C., America, 42pp.

Todoriki, M., T. Furumura, and T. Maeda (2017). Effects of sea water on elongated duration of ground motion as well as variation in its amplitude for offshore earthquakes, *Geophys. J. Int.* **208,** 226–233, doi: 10.1093/gji/ggw388.

Tsuji, T., R. Kamei, and R. G. Pratt (2014). Pore pressure distribution of a mega-splay fault system in the Nankai Trough subduction zone: Insight into up-dip extent of the seismogenic zone, *Earth Planet. Sci. Lett.* **396,** 165–178.

Tsuji, T., J. Dvorkin, G. Mavko, N. Nakata, T. Matsuoka, A. Nakanishi, S. Kodaira, and O. Nishizawa (2011). $V_P/V_S$ ratio and shear-wave splitting in the Nankai Trough seismogenic zone: Insights into effective stress, pore pressure, and sediment consolidation, *Geophysics* **76,** WA71–WA82, doi: 10.1190/1.3560018.

Tsuno, S., and K. Kudo (2008). Estimation of *S*-wave velocity structures in the southern area of Shizuoka Prefecture by analyzing array data of long-period microtremors and strong motions, *BUTSURI-TANSA* **61,** 499–510 (in Japanese with English abstract).

Viens, L., H. Miyake, and K. Koketsu (2015). Long-period ground motion simulation of a subduction earthquake using the offshore-onshore ambient seismic field, *Geophys. Res. Lett.* **42,** 5282–5289, doi: 10.1002/2015GL064265.

Wald, D. J., and R. W. Graves (2001). Resolution analysis of finite fault source inversion using one- and three-dimensional Green's functions 2. Combining seismic and geodetic data, *J. Geophys. Res.* **106,** 8767–8788.

Wessel, P., and W. H. F. Smith (1998). New, improved version of Generic Mapping Tools released, *Eos Trans. AGU* **79,** 579.

Watanabe, T., M. Nagano, and K. Kato (2014). Influence of accretionary wedge along the Nankai Trough and earthquake locations on long-period ground motions in Tokyo, *J. Struct. Constr. Eng. Trans. AIJ* **79,** 701–710 (in Japanese with English abstract).

Yagi, Y. (2004). SE off Kii Peninsula earthquakes of September 5, 2004, http://iisee.kenken.go.jp/staff/yagi/eq/Japan20040905/Japan20040905_1−j.html (last accessed Dcember 2016, in Japanese).

Yamada, N., and T. Iwata (2005). Long-period ground motion simulation in the Kinki area during the $M_J$ 7.1 foreshock of the 2004 off the Kii Peninsula earthquakes, *Earth Planets Space* **57,** 197–202.

Yamada, Y., and Y. Yamanaka (2012). 3D *S*-wave velocity model of Kanto basin for long-period ground motion simulation with special focus on treatment of shallow near surface part, *BUTSURI-TANSA* **65,** 139–150 (in Japanese with English abstract).

Yamamoto, Y., H. Takenaka, K. Hirata, and T. Watanabe (2004). Estimation of broadband ground motion at ocean-bottom strong-motion stations for the 2003 Tokachi-oki earthquake, *2004 AGU Fall Meeting*, San Francisco, America, 13–17 December 2004, Abstract S34A–08.

Yamanaka, Y. (2004). Source rupture processes of the 1944 Tonankai earthquake and the 1945 Mikawa earthquake, *Chikyu Monthly* **26,** 739–745 (in Japanese).

Yao, H., P. Gouedard, J. A. Collins, J. J. McGuire, and R. D. van der Hilst (2011). Structure of young East Pacific Rise lithosphere from ambient noise correlation analysis of fundamental- and higher-mode Scholte-Rayleigh waves, *C. R. Geosci.*, **343,** 571–583.

Yokota, Y., T. Ishikawa, S. Watanabe, T. Tashiro, and A. Asada (2016). Seafloor geodetic constraints on interplate coupling of the Nankai Trough megathrust zone, *Nature*, **534,** 374–377, doi: 10.1038/nature17632.

Yoshida, S., K. Koketsu, B. Shibazaki, T. Sagiya, T. Kato, and Y. Yoshida (1996). Joint

inversion of near- and far-field waveforms and geodetic data for the rupture process of the 1995 Kobe earthquake, *J. Phys. Earth*, **44,** 437–454.

Yoshimoto, K., and S. Takemura (2014). A study on the predominant period of long-period ground motions in the Kanto basin, Japan, *Earth Planets Space* **66,** 100, doi: 10.1186/1880–5981–66–100.

Yoshimura, C., Y. Yamamoto, and Y. Hisada (2008). Long-period ground motion simulation of 2004 off the Kii Peninsula earthquakes and prediction of future M8 class earthquakes along Nankai Trough subduction zone, south of Japan island, *Proc. of the 14th World Conf. on Earthq. Eng.*, Beijing, China, 12–17 October 2008, Paper No. S10–048.

# Acknowledgement

First of all, I greatly thank Professor Kazuki Koketsu for his advice, discussion, and inspiring me to study on waveform inversions and accretionary wedges. I express my sincere appreciation to my defense committee members: Professors Takashi Furumura and Masanao Shinohara, and Associate Professors Ryosuke Ando and Kiwamu Nishida.

I appreciate Associate Professor Hiroe Miyake's countless and helpful advice, encouragement, and discussion.

I thank Mr. Hiroaki Kobayashi for giving a lot of advice and inspiration to my analyses, Dr. Kazuhito Hikima for his kind advice about waveform inversions, and Dr. Yasushi Ikegami for allowing me to use his code for 3-D ground motion simulations. I also thank all members of Koketsu laboratory and the Strong Motion and Tsunami Seismology Seminar for assistance and comments.

I give special thanks to Mr. Yamato Horikawa for giving me a lot of mental support. I also thank my family for financial support.

The digitized seismograms of the 1944 Tonankai earthquake were provided by Associate Professor Yoshiko Yamanaka and Dr. Gene A. Ichinose. Most waveform data were obtained from the National Research Institute for Earth Science and Disaster Resilience (NIED), the Japan Agency for Marine-Earth Science and Technology (JAMSTEC), and the Japan Meteorological Agency (JMA). A large part of 3-D ground motion simulations in this study were performed using the Fujitsu PRIMEHPC FX10 System (Oakleaf-FX) in the Information Technology Center at the University of Tokyo. Figures were drawn using the Generic Mapping Tools (Wessel and Smith, 1998) version 4.5.5.